Article:
Wilson, Katherine M., Jagger, Alistair M, Walker, Matthew et al. (5 more authors) (2018) Glycans modify mesenchymal stem cell differentiation to impact on the function of resulting osteoblasts. Journal of Cell Science. jcs209452. ISSN 0021-9533

https://doi.org/10.1242/jcs.209452

Glycans modify mesenchymal stem cell differentiation to impact the function of resulting osteoblasts

Katherine M. Wilson, Alistair M. Jagger, Matthew Walker, Estere Seinkmane, James M. Fox, Roland Kröger[1], Paul Genever, Daniel Ungar[2]

Departments of Biology and [1]Physics, University of York, York, YO10 5DD, United Kingdom

[2]Correspondence to:

Daniel Ungar

Email: dani.ungar@york.ac.uk, Tel: +44-1904-328656

Summary Statement

Both *N*- and O-glycan processing modulate MSC differentiation early during osteogenesis to influence mineral formation. Inhibition of *N*-glycan processing increases mineralization by influencing PI3K signalling and collagen 1A expression.

JCS Advance Online Article. Posted on 11 January 2018

Abstract

Glycans are inherently heterogeneous, yet glycosylation is essential in eukaryotes and glycans show characteristic cell type dependent distributions. Using an immortalized human mesenchymal stromal cell (MSC) line model we show that both *N*- and O-glycan processing in the Golgi functionally modulate early steps of osteogenic differentiation. Inhibiting O-glycan processing in the Golgi prior to the start of osteogenesis inhibited the mineralization capacity of the formed osteoblasts three weeks later. In contrast, inhibition of *N*-glycan processing in MSCs altered differentiation to enhance mineralization capacity of the osteoblasts. The effect of *N*-glycans on MSC differentiation was mediated by the phosphoinositide-3-kinase (PI3K)/Akt pathway through reduced Akt phosphorylation. Interestingly, by inhibiting PI3K during the first two days of osteogenesis we were able to phenocopy the effect of inhibiting *N*-glycan processing. Thus modulating the functional outcome of differentiation through glycan processing provides another layer of regulation. Glycan processing can thereby offer a novel set of targets for many therapeutically attractive processes.

Keywords:

glycan processing; hydroxyapatite; kifunensine; osteogenesis; PI3K signalling

Introduction

Glycosylation is a ubiquitous posttranslational modification of proteins. Glycans synthetized in the eukaryotic secretory pathway are credited with several examples of modifying specific protein functions, such as the folding, stability and targeting of secretory proteins (Ihrke et al., 2001; Kingsley et al., 1986). Moreover, the importance of glycan processing for the development of complex life is well recognized, given many described developmental defects caused by aberrant glycosylation (Hennet and Cabalzar, 2015). It is also well documented that protein-linked glycan compositions undergo large changes during differentiation events in mammals, thereby giving rise to large cell-type dependent variations in glycan profiles (An et al., 2012; Hamouda et al., 2013; Hasehira et al., 2012; Wilson et al., 2016). However, it is largely unknown if these glycosylation changes are functionally contributing to the differentiation process itself, potentially altering the function of the differentiated cells, or are mere bystanders of cell-specification processes.

Differences in glycosylation are established during glycan processing mainly in the Golgi apparatus. The inherent heterogeneity of glycosylation, ensured by the 200+ enzymes that add or remove monosaccharides, thereby makes it difficult to assess the contributions of specific glycans or even glycan types to cellular function. Glycans can be lipid- or protein-linked, the latter classified as O-linked if the glycan is attached to Ser/Thr or *N*-linked for Asn-attached glycans. For *N*-glycans a mannose-rich chain – called an oligomannose glycan – is established in the endoplasmic reticulum (ER) and trafficked with its carrier protein to the Golgi apparatus. Here mannoses are trimmed in the *cis*/*medial*-Golgi before addition of *N*-acetylglucosamine (GlcNAc) residues in the *medial*-Golgi. The added GlcNAc residues initiate branches that form the basis for hybrid and complex *N*-glycans. Complex *N*-glycan chains contain galactose, fucose and lactosamine modifications, and are commonly terminated with sialic acids. If initial mannose trimming by the enzyme mannosidase I is inhibited, only oligomannose *N*-glycans will be present (Elbein et al., 1990). In contrast, inhibition of the mannosidase II enzyme will favour hybrid glycan formation (Gross et al., 1983). In mammals O-glycans are largely divided into mucin-types and the more specialized glycosaminoglycans, although other minor types are also present. Details of mucin type O-glycan processing are less well understood than for *N*-glycans. This is initiated by an *N*-acetylgalactosamine (GalNAc) residue, which is elaborated with galactose and GlcNAc in branched arrangements to form one of four core structures (Ungar, 2009). These core structures are further modified by the addition of lactosamine, sialic acid and fucose

modifications, similar to but often distinct from *N*-glycans. The processing of mucin type O-glycans can be inhibited by GalNAc analogues that competitively inhibit the addition of monosaccharides downstream of the initial GalNAc (Kuan et al., 1989). Besides the expression and activities of glycan processing enzyme subsets, their localization within the Golgi apparatus also markedly influences glycan profiles. Enzyme localization is determined through vesicular sorting, mediated by the conserved oligomeric Golgi (COG) tethering complex (Miller and Ungar, 2012). COG mutations have been shown to result in glycosylation defects in various organisms (Bailey Blackburn et al., 2016; Belloni et al., 2012; Kingsley et al., 1986; Struwe and Reinhold, 2012; Whyte and Munro, 2001; Wu et al., 2004) by affecting multiple different glycosylation pathways (Kingsley et al., 1986; Spessott et al., 2010). This is due to the mis-sorting of Golgi-proteins (Oka et al., 2004), which affects both their final locations and steady state levels (Fisher and Ungar, 2016).

There is limited evidence for a functional contribution of glycans to the differentiation process, and this is restricted to terminal glycan modifications. For example, glycan features such as lactosamine and fucosylation have been implicated in the self-renewal of stem cells, and by implication in the prevention of differentiation (Hamouda et al., 2013; Kumar et al., 2013; Sasaki et al., 2011). A particular focus has been on the role of terminal sialic acid. Sialidase treatment was shown to reduce osteogenesis (Tateno et al., 2016) and regulatory T-cell differentiation (Lin et al., 2015). In contrast, sialylation was found to inhibit human embryonic stem cell differentiation (Alisson-Silva et al., 2014). In addition, immune development also involves sialylation that influences major histocompatibility complex binding (Moody et al., 2001).

The differentiation of mesenchymal stem cells (MSCs) is a good model to investigate the contributions of glycans to the differentiation process. The glycan profiles of the stem cells and their progeny have been well documented. For example, in MSCs about 45% of the *N*-glycans are oligomannose with 55% complex, this is altered to 30% oligomannose and 70% complex in osteoblasts (Wilson et al., 2016). Osteoblasts differentiate from MSCs and are responsible for bone generation. MSCs can receive pro-osteogenic signals, as well as anti-adipogenic and anti-proliferative cues, to promote differentiation into osteoblast precursors. Runt-related transcription factor 2 (Runx2) is a key transcription factor that regulates osteogenesis (Ducy et al., 1997). It induces the expression of several osteoblast specific genes, for example α1 collagen and bone sialoprotein (BSP). A large body of work has implicated various signalling pathways in osteogenic differentiation and subsequent

mineralization (Cook and Genever, 2013). In particular, TGF-β signalling (for example through bone morphogenetic protein 2 (BMP2), Lee et al., 2000), Wnt signalling (via Wnt3a, Quarto et al., 2010), and several FGF pathways (Su et al., 2014) all feed into osteogenesis. The involvement of individual pathways is often controversial. For example, the phosphoinositide-3-kinase (PI3K) signalling pathway has been implicated both in promoting (Hamidouche et al., 2009) and antagonizing (Kratchmarova et al., 2005) osteogenesis, dependent on the activation state of the pathway within specific stages of osteogenic differentiation.

Here we find that alteration of either *N*- or O-glycan processing in the Golgi fundamentally influences osteogenic differentiation of an immortalized human clonal MSC line. While inhibiting O-glycan processing inhibited functional osteogenic differentiation, interestingly the inhibition of an early step in *N*-glycan processing altered differentiation to ultimately promote more mineralization in the formed osteoblasts. This change in differentiation is due to altered PI3K mediated signalling in the first days of osteogenic differentiation, implicating protein-linked glycans in the fine-tuning of signalling to influence cellular differentiation.

Results

Genetic disruption of the glycosylation synthesis pathway alters the N- *and O-glycan profile of hTERT-MSCs.*

Altering glycosylation enzyme localization in the Golgi by interfering with vesicular sorting has the potential to broadly perturb several different glycan biosynthetic pathways. This can be used to globally assess the function of glycans in a cell biological process. Such a perturbation was achieved by knocking down a subunit of the COG vesicle tethering complex, Cog4, using RNA interference. MSCs exist in a heterogeneous population of bone marrow stromal cells, including partially differentiated osteoprogenitors, from which they are hard to distinguish. To help circumvent any issues associated with MSC heterogeneity, here we used a highly characterized human clonal MSC line. Y101 cells were previously immortalised by transduction with human telomerase reverse transcriptase (hTERT), and represent a reproducible model of *in vitro* differentiation (James et al, 2015). Importantly, glycosylation of the Y101 line is unlikely to be altered due to immortalization, as comparison of three independent hTERT-MSC clones with different phenotypes (Y101, Y201, Y202) has shown no significant differences in their *N*-glycan profiles (Wilson et al., 2016). hTERT-

MSC Y101 clones expressing one of two different Cog4-specific shRNAs were generated (Cog4KDshRNA1 and Cog4KDshRNA2). Both Cog4 knock-down MSC lines have over 60% reduction in Cog4 protein levels compared to wild-type (WT) controls (Fig 1A). Glycosylation alterations were first investigated using lectin staining quantified by flow cytometry. As expected, both the sialic acid binding *Sambucus Nigra* Lectin (SNA) and the GalNAc binding *Vicia Villosa* Lectin (VVL) showed reduced staining in Cog4 knock-down lines (Fig 1B and Suppl. Fig 1). These indicate changes in mucin type O-glycan and likely also *N*-glycan biosynthesis. A recent report with a more detailed description of the changes in the O-glycan profile of Cog4KD MSCs confirms these differences, indicating a global alteration of mucin type protein O-glycosylation (Skeene et al., 2017). To identify more specific changes in *N*-glycan processing, Cog4 knock-down hTERT-MSCs were harvested, and total cellular *N*-glycans isolated by filter-aided *N*-glycan separation (FANGS, Abdul Rahman et al., 2014). Following permethylation the glycans were analyzed by MALDI-TOF mass spectrometry. The *N*-glycan profile of Cog4 knock-down cells is highly similar to WT hTERT-MSCs (Fig 1C, compared here to the published (Wilson et al., 2016) WT and osteoblast spectra). No significant differences are seen when individual glycans of >0.02% abundance are quantified (Suppl. Table 1), or when the relative abundance of the different glycan classes is calculated (Suppl. Fig 2). The abundance of higher-mass complex glycans above about 2700 m/z is visibly lower in the Cog4 knock-down spectrum. However, this difference is not statistically significant when the relative abundances from multiple repeats are summed up. Interestingly though, the same class of higher-mass glycan species dominates the profile of osteoblasts differentiated from the hTERT-MSCs (Wilson et al., 2016 and Fig 1C). Given the successful alteration of protein glycosylation in MSCs, *in vitro* osteogenesis was used as a model to assess the impact of glycan biosynthesis modulation on cell differentiation.

Glycosylation impacts on the mineralization behaviour of differentiating osteoblasts

As previously reported, Y101 hTERT-MSCs cultured in osteogenic medium for 3 weeks undergo differentiation into osteoblasts, and produce hydroxyapatite mineral deposits (James et al., 2015). At the same time there is a dramatic change in the *N*-glycan profile of the cells (Wilson et al., 2016), which could serve as MSC-specific markers. To assess if the glycans are also functionally important during differentiation, the glycosylation defective Cog4

knock-down Y101 cells were subjected to differentiation. After culturing in osteogenic medium for three weeks, WT cells showed productive osteogenic differentiation, as visualized by alizarin red staining (Fig 2A), pink alkaline phosphatase (ALP) staining, and numerous von Kossa-stained brown dots representing mineralized calcium phosphate deposits (Fig 2B). In contrast, the Cog4 knock-down lines showed minimal alizarin red staining and very few von Kossa stained deposits, attesting of largely failed mineralization, although ALP staining was still present (Fig 2A and 2B top right). Quantification of the eluted alizarin stain confirmed the strong mineralization defect (Fig 2A graph).

Cog4 depletion alters a number of different glycosylation pathways (Fisher and Ungar, 2016), including *N*-glycan, O-glycan (Kingsley et al., 1986) and glycolipid (Spessott et al., 2010) biosynthesis. We next sought to address which of these specifically affect differentiation of the Y101 hTERT-MSCs. Cells were therefore cultured in the presence of various glycan biosynthesis inhibitors and their differentiation assessed. We have previously published that inhibiting complex *N*-glycan biosynthesis using swainsonine did not affect mineralization (Wilson et al., 2016). Inhibiting glycolipid biosynthesis using *N*-butyldeoxynojirimycin (NB-DNJ, Fig 2B middle left) had no effect on ALP and von Kossa staining either. To investigate further the contributions of the *N*-glycan processing pathway, the mannosidase I inhibitor kifunensine was used, which completely inhibits *N*-glycan processing in the Golgi, but has no effect on the proliferation rate of cells (Suppl. Fig 2A, B, C, E). Interestingly, addition of kifunensine during osteogenesis resulted in visibly more abundant von Kossa staining, indicating increased mineralization (Fig 2B middle right). These observations imply that complex and hybrid *N*-glycans and glycolipid glycans are not responsible for the observed defects in Cog4 depleted cells. In contrast, inhibiting O-glycan biosynthesis phenocopied the effects of Cog4 depletion by inhibiting mineralization. Differentiating cells in the presence of the proteoglycan sulfation inhibitor $NaClO_3$ (Fig 2B bottom left) or the mucin type O-glycan synthesis inhibitor benzyl-O-GalNAc (BG, Fig 2B bottom right), lead to positive pink ALP staining, without significant amounts of brown von Kossa staining. Inhibiting the processing of mucin type O-glycans had again no effect on cell proliferation (Suppl. Fig 2B, D, E), although the GAG sulfation inhibitor $NaClO_3$ at the used concentration did slow down the proliferation of cells upon prolonged incubation (Suppl. Fig 2F).

While mineralization is a clear functional consequence of osteogenic differentiation, its absence does not necessarily mean a complete ablation of the osteogenic differentiation programme. As another test, real-time qPCR assays were performed investigating the expression levels of three mRNAs as markers of osteogenic differentiation (Kulterer et al., 2007): the transcription factor Runx2, the growth factor BMP2, and the crystal nucleator BSP. Despite observing a clear loss of mineralization in both Cog4KD lines there was little difference in the expression patterns of Runx2 between WT and the shRNA1 line. While the fold-changes for shRNA2 are different, the trends are consistent with both shRNA1 and WT (Fig 2C). Levels of BMP2 and BSP mRNA did not show sharp changes at 21 days in shRNA treated cells as seen in WT, and the effects were opposite for the two markers (higher in WT for BSP, lower in WT for BMP2, Fig 2C top row). Even less different compared to controls were BG treated cells, as no differences in the levels of the tested markers could be seen (Fig 2C middle row). For the drug treatments we investigated two further genes, the transcription factor osterix as an additional early marker, and the crystallization factor osteocalcin as a late marker (Kulterer et al., 2007). While neither of these showed a statistically significant difference compared to the untreated controls, the trend in the osteocalcin gene expression was consistent with the lack of mineralization (Suppl. Fig 3). Indeed, comparing samples on separate individual days, the decrease in osteocalcin expression on day 7 and 28 was statistically significant. This change in osteocalcin expression could be responsible for the reduced mineralization seen with BG, something future studies could address. Surprisingly, following kifunensine treatment, which enhanced mineralization (Fig 2B), the mRNA levels of Runx2, BSP and osteocalcin were consistently lower throughout osteogenesis than in control cells. BMP2 expression did increase in-line with the control after 7 days, but failed to reach the maximal induction at day 14 (Fig 2C bottom row). Collectively these qPCR-based findings may imply that the main impacts of Cog4 depletion, as well as kifunensine- and BG-treatments were on the process of mineralization rather than differentiation *per se*, but they do not rule out a direct involvement in controlling aspects of cell differentiation.

N- *and O-glycosylation directly impact on MSC differentiation*

The results presented so far implicate both *N*-glycan and mucin-type O-glycan processing in osteoblast functionality, but do not provide evidence for their involvement in differentiation itself. We noticed that most inhibitors had to be added for a period of 48 h prior to differentiation for effects to be observed, while shorter pre-treatments had no effect. We reasoned that specific glycan types could be generated or depleted in this pre-differentiation period, which could prime the cells for altered differentiation and following this, osteoblast activity. To test if specific glycan types are involved in early differentiation decisions, cells were treated with glycosylation inhibitors for 48 h prior to addition of osteogenic medium. Osteogenic differentiation was then continued in the absence of glycosylation inhibitors for 21 days.

Inhibiting proteoglycan sulfation is known to be important for osteogenesis (Kumarasuriyar et al., 2009, and Fig 2B). Yet pre-treatment of Y101 MSCs with the sulfation inhibitor $NaClO_3$ was not sufficient to influence mineralization in the same way as continuous treatment. Pre-treated cells showed ALP and von Kossa staining indistinguishable from controls (Fig 3A second row). In contrast, BG and kifunensine pre-treatments (Fig 3A third and fifth rows) had the same effect on decreasing and increasing mineralization respectively, as continuous treatment with the inhibitors. Given the markedly reduced expression of osteogenic marker mRNA levels during continuous kifunensine treatment, we wondered if this effect is also recapitulated during the pre-treatment-only regime. Indeed, the pattern of expression levels of Runx2, BMP2, and BSP mRNAs were very similar in kifunensine pre-treated and continuously treated hTERT-MSCs (Fig 3B), and similar results were obtained for osteocalcin and osterix as well (Suppl. Fig 3). Together the mineralization and qPCR data indicate altered MSC osteogenic differentiation when protein glycosylation is modified.

To determine the epistatic relationship between the *N*- and O-glycan processing pathways during MSC differentiation, hTERT-MSCs were co-treated with kifunensine and BG for 48 hours in basal medium, prior to subjecting them to osteogenic medium in the absence of the glycan processing drugs for 21 days (Fig 3A seventh row). The lack of positive von Kossa staining at the end of the 21 day differentiation following dual treatment indicates that O-glycan processing is dominant over *N*-glycan processing. Interestingly,

treatment of Cog4KD hTERT-MSCs with kifunensine also did not rescue the mineralization defect (Fig 3A bottom row) suggesting that disruption of the O-glycan synthesis pathway could likely contribute to the altered MSC phenotype caused by Cog4-knock-down.

Enhancement of mineralization does not alter the ultrastructure of the formed mineral

The enhanced mineralization potential of kifunensine-treated MSCs could be particularly interesting from a therapeutic angle. However, the reduced levels of established osteogenic markers observed by qPCR during the same differentiation experiments could indicate a non-conventional differentiation process, which could potentially cause abnormal or artefactual mineral formation. ALP is important for mineralization as it generates the phosphate required for hydroxyapatite. Histological staining did show ALP to be present in kifunensine-treated cells (pink staining in ALP/von Kossa stained images of Fig 2B and 3A), and this was confirmed by western blot analysis (Suppl. Fig 4A). On the blot the level of ALP, as well as its apparent molecular weight are lower upon continuous kifunensine treatment, but both of these are reverted to normal in samples that have only been pre-treated with the drug. Importantly though, total enzymatic activity is not significantly different in continuously kifunensine treated compared to control samples (Suppl. Fig 4B). A possible explanation for this is that altered glycosylation may impact on ALP enzymatic activity. In conclusion, it is not simply enhanced phosphate generation that is responsible for the increased mineralization in kifunensine-treated cells. Key for the formation of mineral with similar properties to that naturally formed in bone is the control of hydroxyapatite organisation through collagen fibrils. Importantly, further real-time qPCR analysis of kifunensine pre-treated and continuously treated hTERT-MSCs revealed that collagen type I is significantly upregulated by both treatments (Fig 4A), implicating a potential physiological route for increased mineralization.

Collagen type I is a major constituent of bone, and mutations to type I collagen are associated with the brittle bone disease osteogenesis imperfecta (Sykes et al., 1986). Importantly, apatite nanocrystals nucleate within the collagen gap regions to form an aligned arrangement parallel to the collagen fibrils (Wang et al., 2012). This was investigated using bright-field transmission electron microscopy to characterize the size and shape of the apatite crystals, and selected area electron diffraction (SAED) to unambiguously identify the apatite mineral. High magnification transmission electron micrographs were collected of unstained

thin sections following resin-embedding of both kifunensine pre-treated and control MSCs following three weeks of osteogenesis. The appearance of the mineral covered areas was very similar between kifunensine treated and untreated samples apart from a generally higher density of the mineral in the drug treated ones (Fig 4B). The form and size of the needle shaped hydroxyapatite crystals was measured as 5.40±0.80 nm (n=15) for control and 5.14±1.16 nm (n=17) following kifunensine treatment. This is in good agreement with the approximately 5 nm width reported for hydroxyapatite crystals in bone specimens (Rubin et al., 2003). To ascertain that the observed crystals following kifunensine treatment are *bona fide* apatite crystals, and have the same crystal form as the ones found in bone, SAED experiments were carried out. These showed a strong 002 diffraction ring with a pattern typical of apatite (Fig 4C, cf. Chatzipanagis et al., 2016). Discontinuity of the 002 reflection in the diffraction pattern can determine co-alignment of the apatite nanocrystals, a feature typically found in bone (Chatzipanagis et al., 2016; Rubin et al., 2003). This is generally a difficult experiment in a 2D tissue culture model, as the amount of deposited mineral is usually not sufficient to observe directional bias of the crystals. However, the high density of the mineral deposits generated by kifunensine treated cells allowed us to observe an incomplete 002 ring. As expected, this effect is more clearly visible in the included diffraction pattern of a bone sample due to the higher amount of ordered mineral in bone compared to the *in vitro* cell model (Fig 4C, compare top and bottom half). This indicates that in kifunensine treated cells crystal co-orientation starts to align with that of the collagen fibrils generally regarded as the sites of nucleation and crystal growth in bone (Weiner and Traub, 1992). These observations suggest that kifunensine treatment increases collagen type 1 expression, thereby facilitating the generation of mineral deposits that possess the correct structure and orientation bias as required for bone formation.

Identifying the signalling pathway linking N-*glycan processing and osteogenesis*

The results so far suggest that kifunensine acts early in the MSC osteogenic differentiation process. Given that the extracellular portions of signalling pathways are usually mediated by glycoproteins, we wondered whether the effects of kifunensine treatment could be attributed to a particular signalling pathway. MSC proliferation and osteogenic differentiation have been associated with several major signalling pathways, including Wnt/β-catenin, TGFβ-BMP/Smad and tyrosine kinase receptor mediated (e.g. FGFR)

pathways. We compared the activation status of these pathways in the first few days of MSC osteogenic differentiation in the presence of a 48 h pre-treatment with kifunensine, BG and both inhibitors, or in the absence of a drug treatment. We reasoned that the pathway responsible for the mineralization enhancing effects of kifunensine should have an altered response upon kifunensine pre-treatment, when compared to untreated or BG pre-treated samples. As expected for Wnt signalling following the induction of osteogenesis, active β-catenin levels did increase, but there was no marked difference between the various treatments (Suppl. Fig 5A). Similarly, phosphorylation of the MAP kinase Erk was not markedly different upon kifunensine treatment when compared to untreated or BG treated osteogenic samples (Suppl. Fig 5B). Although treatment with both inhibitors did lead to reduced Erk activation after seven days (Suppl. Fig 5B last lane), this was not further investigated given the lack of difference between the other three treatment groups. Moreover, investigating the TGF-β pathway, we could not detect significant levels of phospho-Smad2/3 under any of the treatment conditions.

To test for receptor tyrosine kinase signalling, the abundances of phosphotyrosine (pTyr) containing proteins were compared between the treatment groups during the first week of osteogenesis (Fig 5A.). While there are differences in the overall intensity of pTyr staining over time, which are independent of the applied drug treatment, the ratio of the two most intense bands seen between the 100 and 150 kDa molecular weight markers is specifically altered. At day two of differentiation in the kifunensine treated sample the lower band of the doublet decreases in intensity relative to the upper band (Fig 5A, B). Although this change was not statistically significant, we decided to follow up on this clear trend. We speculated that the lower of these two bands could represent the p110 subunit of phosphoinositide-3-kinase (PI3K). This speculation is somewhat substantiated by findings of Kratchmarova and colleagues; based on the molecular weights and related observations about platelet derived growth factor (PDGF)-induced tyrosine-phosphorylated proteins in MSCs (Kratchmarova et al., 2005). Interestingly, that study also implicated the PI3K pathway in the PDGF-dependent inhibition of osteogenesis (Kratchmarova et al., 2005).

Lowered PI3K phosphorylation would lead to a change in the levels of phosphorylated Akt, a downstream effector of PI3K (Franke et al., 1995). Total Akt levels as well as the phosphorylation state of the two main sites (Thr308 and Ser 473) both change over the course of the first week of differentiation even in the absence of any other treatments (Fig 6 – cf no treatment). Yet when the phosphorylation states were carefully quantified and normalized to

both total Akt and the housekeeping protein tubulin, a change upon kifunensine treatment did emerge. Both the Thr308 and the Ser473 residues of Akt had a lower level of phosphorylation two days after the start of differentiation in kifunensine treated hTERT-MSCs compared to the untreated and BG treated cells (Fig 6). In the case of Akt Thr308 phosphorylation this difference even persisted at the seven day time point. None of the differences were statistically significant after only four experimental repeats. Given the stronger effect on pSer473 phosphorylation at two days we increased the sample size for this phosphorylation site to six, which indeed showed a statistically significant reduction in phosphorylation after two days specifically in the kifunensine pre-treated sample. This supports the hypothesis that inhibition of PI3K signalling could be the mechanism by which kifunensine treatment alters osteogenesis and enhances consequent mineralization.

Based on the above observations the PI3K inhibitor wortmannin was used to attempt to phenocopy the effects of kifunensine. We first verified that 100 nM wortmannin indeed resulted in a significant reduction of Akt phosphorylation in the presence of osteogenic medium (Suppl. Fig 6). We then reasoned that the 48 h pre-treatment with the glycosidase inhibitor would have altered the glycosylation state of signalling components by the time differentiation was initiated. This then would have had a transient effect on the signalling machinery during the first few days of differentiation. Therefore, wortmannin was applied during the first two days of differentiation onto MSCs that were not treated with kifunensine, and following three weeks of differentiation the cells stained with alizarin red to allow quantification of the formed mineral deposits. Treating Y101 cells with 100 nM wortmannin during the first two days of differentiation significantly increased alizarin staining, and by inference mineralization (Fig 7), similarly to kifunensine treatment.

Discussion

Our study provides evidence for the functional involvement of Golgi-based glycan processing in the early steps of cellular differentiation. Restricting mannosidase I inhibition to the two days prior to the start of differentiation increased mineral formation. It is evident that the effect of kifunensine pre-treatment is transient, for example the altered glycosylation of ALP seen upon continuous treatment disappears when only pre-treatment is applied (Suppl. Fig 3A). These data argue that it is indeed the differentiation programme itself that glycosylation influenced early on rather than merely affecting the molecular function of the factors responsible for mineral formation, which themselves appear later during

differentiation (Cook and Genever, 2013). Given that swainsonine treatment did not alter the mineralization behaviour of osteoblasts (Wilson et al., 2016) but kifunensine treatment significantly increased it, it is not simply the lack of complex glycans driving the enhancement. Similarly, it is not just the lack of terminal sialylation, an alteration that has previously been implicated in differentiation events (Alisson-Silva et al., 2014; Moody et al., 2001), which drives this differentiation mechanism. Future studies will have to address exactly which *N*-glycan species are needed for enhanced differentiation, although this could well involve a range of glycans. The *N*-glycan profiles of three different hTERT-MSC lines are virtually indistinguishable (Wilson et al., 2016), while their differentiation characteristics are clearly different (James et al., 2015). Therefore, *N*-glycans almost certainly play a modulatory role for differentiation rather than a deterministic one. Interestingly, a second type of glycan processing, that of mucin type O-glycans, also modulates differentiation, in this case inhibiting the generation of functional osteoblasts that are capable of mineral deposition. This is also due to an early event, as in the case of mannosidase I inhibition.

Which molecular factors could be responsible for the effects of altered glycan processing on differentiation of this model cell system? *N*-glycan processing has been shown to influence the signalling behaviour of receptors such as EGFR (Sato et al., 2001) and cytokine receptors (Partridge et al., 2004). In these cases the effect of the glycan is on receptor endocytosis, and mostly depends on complex *N*-glycan branching (Lau et al., 2007). This mechanism by itself is less likely to be relevant given the differences observed between inhibiting mannosidase I and II, which both eliminate complex glycan branching. In contrast, ICAM-1-mediated signalling was significantly altered by limiting its glycans to an oligomannose form, which directly influenced the interactions with intracellular partners (Scott et al., 2013). Such a mechanism could potentially be more relevant in our system. The effects of glycosylation on receptor/growth factor function are generally conveyed by lectins that specifically bind to the presented glycans. Recently the lectin Clec11a/osteolectin was shown to promote osteogenesis of MSCs (Yue et al., 2016). The consensus carbohydrate binding motif of Clec11a does not conform to either a galactose specific Gln-Pro-Asp nor a mannose specific Glu-Pro-Asn sequence (Drickamer, 1992). This makes it difficult to implicate Clec11a in a mechanism of kifunensine-dependent increased mineralization before its monosaccharide specificity can be investigated.

While pinpointing the specific glycoprotein(s) responsible for mediating the consequences of altered glycan processing is beyond the scope of this study, it was possible to delineate affected signalling pathways and their outputs. Using the clonal Y101 MSC line, rather than a variable mixed MSC population, has thereby the advantage of well-defined differentiation characteristics (James et al., 2015) in order to study fundamental cell biological questions. It is interesting though that most of the tested qPCR markers do not follow the trend expected by the functional output of mineralization. For example, O-glycan modulation, which suppresses mineralization, has no effect on Runx2, BMP2, BSP and osterix. In contrast, kifunensine in part suppresses the upregulation of these markers although it promotes increased mineralization. The late marker osteocalcin could potentially explain the effects of O-glycan inhibition, as it does show a trend for lower expression, but it again cannot explain the effects of kifunensine. The much reduced upregulation of the markers in the case of kifunensine could imply a shift of biosynthetic capacity, to be used for example to generate collagen that we did find to be upregulated. We propose the rather speculative possibility that in Y101 cells collagen levels are rate-limiting for mineralization whereas other differentiation induced factors are not. In line with this reasoning, ALP activity is not limiting here for increased mineralization. The rebalancing of resources (from Runx2/BMP2/BSP towards collagen) through altered glycan processing could tie in with the established role of the glycan processing machinery in translating the nutrient state of the cell into growth cues (Lau et al., 2007).

As Y101 cells are a subclone of MSCs, it is difficult to assess the overall importance of the uncovered effects on the PI3K pathway for osteogenesis in a primary MSC mixture. Both pro- and anti-osteogenic effects of PI3K signalling have previously been reported. These have investigated PI3K signalling from different angles. For example, PI3K was described as an essential pro-osteogenic signalling component downstream of BMP2 (Ghosh-Choudhury et al., 2002), Wnt3a (Ling et al., 2010) and integrin (Hamidouche et al., 2009) signalling. In contrast, PI3K inhibition was shown to release the inhibition of osteogenesis conveyed by PDGF activation (Kratchmarova et al., 2005). Thus the PI3K pathway could act either positively or negatively on osteogenesis, dependent on the circumstances. It is also apparent that the MAPK pathway, which often shares cell surface receptors with the PI3K pathway can be regulated in opposite ways or even independently of PI3K (Yokota et al., 2014). What is common in all previous studies though, is that they investigated PI3K signalling throughout

the studied differentiation program. We can now add a further piece to this puzzle by showing that a short transient inhibition of PI3K at the start of osteogenesis can alter differentiation to ultimately enhance mineralization in the Y101 MSC line. This modulatory effect of PI3K signalling is in fact a likely conduit for glycans to influence differentiation. Thus fine tuning the balance in signalling pathways is something that altered glycoforms can potentially accomplish. While these processes are limited at the moment to our model cell line, representing a subpopulation of MSCs, they could still be important in the context of varying glycosylation between individuals, in diseases or aging. Interestingly, many individuals suffering rare congenital glycosylation disorders have symptoms consistent with bone malformations (Coman et al., 2008).

Materials and Methods

Chemicals were from Sigma and cell culture reagents from Invitrogen unless otherwise indicated.

Cell culture, osteogenesis and inhibitor treatments

Y101 hTERT-MSCs (James et al., 2015) were cultured in basal medium (Dulbecco's Modified Eagle Medium (DMEM, high glucose, pyruvate, no glutamine) supplemented with 10% fetal bovine serum (FBS), 1% Penicillin/streptomycin and 1% Gluta-Max-I). To induce osteogenic differentiation basal medium was supplemented with 50 µg/ml ascorbic acid, 5 mM β-glycerophosphate and 10 nM dexamethasone, and changed every 3-4 days for the indicated period.

Cog4 knock-down hTERT-MSCs were generated using MISSION shRNA lentiviral particles (Sigma, TRCN0000180098 designated shRNA1 and TRCN0000149947 designated shRNA2) according to the manufacturer's instructions. A multiplicity of infection (MOI) of 1 was used for transduction. Single cell derived clones were selected using 2 µg/ml puromycin. The Cog4 MISSION constructs TRCN0000146949, TRCN0000423404 and TRCN0000443798 were also used but did not result in significant Cog4 knock-down.

For treatments with glycosylation inhibitors (kifunensine (Kif, Santa Cruz Biotechnology, 2 µg/ml), benzyl-2-acetamido-2-deoxy-D-galactose (BG, 2 mM), $NaClO_3$ (25 mM), N-butyldeoxynojirimycin (NB-DNJ, Santa Cruz Biotechnology, 150 µM) cells were cultured in basal medium with addition of the inhibitor for 48 hours before the start of differentiation. Following this treatment the inhibitor was added to osteogenic medium where indicated.

Flow cytometric analysis of lectin binding

All centrifugations were at 450 g for 5 min. Cells were washed twice with phosphate buffered saline (PBS), incubated at 37°C for 10 min with washing buffer (0.2% BSA, 5 mM EDTA in PBS), and detached cells centrifuged. The cells were resuspended in PBS, counted and re-pelleted. All following incubations were at 4°C or on ice. Cells were resuspended in PBS at 10^6 cells/ml, 100µl of the suspension was incubated for 15 min before adding 100 µl lectin in washing buffer and incubating in the dark for 30 min. Following addition of 1ml washing buffer and centrifugation the pellet was resuspended in 100 µl of washing buffer containing 1 µg/ml DAPI for FITC conjugated lectin (Vector Labs) or 5 µg/ml streptavidin-fluorescein (Vector Labs) for biotinylated lectin and incubated in the dark for 5 minutes (DAPI, for FITC-lectin) or 30 min (streptavidin-FITC, for biotin-lectin). Streptavidin-FITC was washed three times before addition of DAPI. Following DAPI incubations 1 ml of washing buffer was added, cells pelleted and resuspended in 400 µl PBS. FACS was performed on a CyAn ADP analyzer (Beckman Coulter) using 405 and 488 nm lasers. Cells were gated for forward- and side-scatter to exclude debris and against 405 nm to select live cells. The count versus log 488 nm fluorescence of live cells was displayed as a histogram and the median fluorescence of this histogram used in comparisons between samples.

Isolation and analysis of N-*glycans by mass spectrometry*

N-glycan samples were prepared using FANGS as described (Abdul Rahman et al., 2014). Glycans were then permethylated and analyzed by mass spectrometry as described (Wilson et al., 2015), using an ultraflex III MALDI-TOF mass spectrometer (Bruker). Spectra

were analyzed using Flex Analysis 3.3 (Bruker) as described (Wilson et al., 2015). In brief, after assignment of a glycan structure to the mono-isotopic peak, the intensities of all corresponding isotopic peaks were summed providing the total peak intensity for a given glycan. Total peak intensities normalized to the sum of all peak intensities within a spectrum were averaged between spectra.

Histological staining

All incubations were at room temperature. Stained wells were imaged with a stereo microscope (Zeiss) or a Leica DMLA upright microscope. Cells for staining were cultured in 24-well plates.

For alkaline phosphatase (ALP)/von Kossa staining, cells were washed twice with PBS before 5 minute incubation in ALP stain solution (0.2 mg/ml naphtol AS-MX in 1% N,N-dimethylformamide, 1 mg/ml Fast Red TR diluted in 0.1 M Tris pH 9.2). Following two PBS washes and fixation (4% paraformaldehyde, 5 min), cells were washed with PBS then with water before incubation in 1% silver nitrate on a light box for 30 minutes. Following this, cells were washed three times with distilled water, incubated for 5 minutes with 2.5% sodium thiosulphate, and following two distilled water washes stored in PBS with 20% glycerol.

For alizarin red staining, following two PBS washes and 15 min fixation in 4% paraformaldehyde cells were washed three times with PBS before 20 min incubation in 40 mM alizarin red S (pH 4.2, reagent filtered and pH adjusted every week). Cells were washed at least five times in tap water until excess stain was removed then air dried. Stain was eluted following imaging by 2 hour incubation in 10% cetylpyridinium chloride and quantified by measuring absorbance at 570 nm. If the absorbance was too high all samples were equally diluted in water and re-measured.

3-(4,5-dimethylthiazol-2-yl)-2,5-diphenyltetrazolium bromide (MTT) assay

For each cell line tested 1200 cells were seeded per well, into 6 wells of a 96 well culture plate. After the indicated number of days culture medium was replaced with fresh medium and 25 µl MTT solution (5 mg/ml in PBS). Plates were then incubated for 3 hours at 37°C in 5% CO_2. MTT solution and medium was removed from wells and 100 µl of 0.04 M HCl in

isopropanol was added to each well. Plates were left to shake at room temperature for 10 minutes to allow for complete solubilisation. Absorbance was then read at 570 nm, and average absorbance (with standard deviation) was used in comparisons.

Analysis of gene expression by real time qPCR

RNA was extracted from cells cultured in a well of a 6-well plate using TRIzol™ (Invitrogen), and suspended in 12 µl nuclease-free water (Hypure, ThermoScientific). RNA was treated with RQ1 RNase-free DNase I (Promega) before using 1 µg for SuperScript II (Invitrogen) catalyzed cDNA synthesis. Real time quantitative PCR was performed using Fast SYBR Green (Applied Biosciences) on a StepOnePlus system (Applied Biosciences) and analyzed using StepOne v2.3 software. Gene expression levels were quantified using the comparative CT (ΔΔCt) method, by normalizing both to the housekeeping gene RPS27a and WT (or untreated) day 0 levels. Primer pairs were:

Runx2: AGTGATTTAGGGCGCATTCCT, GGAGGGCCGTGGGTTCT

BMP2: ACTCGAAATTCCCCGTGACC, CCACTTCCACCACGAATCCA

BSP: GAGGAGGAAGAGGAAGGAAATG, TGGTACTGGTGCCGTTTATG

Osterix: GCC AGA AGC TGT GAA ACC TC, GCT GCA AGC TCT CCA TAA CC

Osteocalcin: AGG GCA GCG AGG TAG TGA AG, AGG GGC AAG GGG AAG AGG AAA G

Collagen 1A1: CAAGAACCCCAAGGACAAGAG, CTTGCAGTGGTAGGTGATGGTC

RPS27a: TGGATGAGAATGGCAAAATTAGTC, CACCCCAGCACCACATTCA

Analysis of protein expression by Western blotting

150 µl sample buffer (5% glycerol, 50 mM Tris pH 6.8, 50 mM DTT, 1% SDS, 0.7 mM bromphenol blue) was used to lyse cells from a well of a 24-well plate. Proteins were separated on 10% gels prior to semi-dry transfer onto polyvinylidene fluoride (PVDF) membrane (ThermoFisher) for 60 minutes at 20V using 48 mM Tris, 39 mM glycine, 20%

methanol, 0.0375% SDS as the transfer buffer. Membranes were blocked using PBS with 0.05% Tween-20, 5% milk (PBSTM) for 1 hour (used 3% BSA instead of milk for blots with the anti-pTyr PY20 antibody), then incubated with primary antibody: affinity purified anti-Cog4 (1:500, Miller et al., 2013), anti-tubulin (1:2000, gift from M.G. Waters, Princeton University), anti-ALP (1:6000, Santa Cruz sc-137213), anti-active β-catenin (1:2000, Millipore 050665), anti-phosphotyrosine (1:1000, used 3% BSA instead of milk, BD Bioscience clone PY20), anti-Akt (1:1000, Santa Cruz sc-1618), anti Akt-pThr308 (1:1000, Cell Signaling 13038), anti-Akt-pSer473 (1:1000, New England Biolabs 4060P) anti-pSmad2/3 (1:500, Santa Cruz sc-11769), anti-pERK (1:4000, R&D Systems AF1018) in PBSTM overnight at 4ºC. Following six 10 minute washes with PBSTM appropriate HRP-linked secondary antibody (1:3000, Bio-Rad) in PBSTM was added for 1 h, the blot washed, and imaged on a GeneGenius Chemi-imager (Syngene) after application of Immobilon HRP substrate (Millipore). Quantification was carried out using ImageJ software.

Electron microscopy

Following three weeks of osteogenesis cells were embedded in Epon Araldite (EMS), and 90 nm thick sections were placed onto 200 mesh carbon coated copper grids. Grids were imaged on a JEOL 2010 TEM operated at 200 kV with a LaB6 crystal as electron source and an UHR lens for an ultimate spatial resolution of 1.9 Å. Selected area electron diffraction patterns to identify the mineral phase were recorded at a camera length of 0.25 m. Crystal width was quantified using ImageJ. The distance between points of half-maximum intensity on lines plotted perpendicular to the crystals' long axis was determined, averaged, and then multiplied by two to give crystal width.

Statistical analysis

Data was analyzed using SigmaPlot 12.3 software. First a normality test (Shapiro-Wilk) and a test of equal variance was performed. For comparison of two groups a Student's T test was used, for more groups a one-way ANOVA test was performed, followed by Holm Sidak post-hoc tests if required. If the data failed the normality or variance tests a Mann-Whitney test was carried out when two groups were compared, and a Kruskal-Wallis One Way Analysis of Variance on Ranks, followed by Dunn's post hoc test was carried out if more

than one group was being compared. Throughout *=p<0.05, **=p<0.01 and ***=p<0.001, ns – non significant.

Acknowledgments

We thank members of the Centre of Excellence for Mass Spectrometry at the University of York, in particular Jane Thomas-Oates, Jerry Thomas and Adam Dowle for help with mass spectrometry. The imaging and genomics facilities of the Bioscience Technology Facility helped with microscopy and qPCR, and we are particularly indebted to Meg Stark for help with EM samples. We thank Martin Lowe (University of Manchester) for helpful comments on the manuscript. This work was supported by an EPSRC funded studentship (supporting KMW) awarded to PG and DU, and by the Arthritis Research UK Tissue Engineering Centre (19429).

Author Contributions

KMW, PG and DU designed the study, analysed the data and wrote the manuscript. KMW performed the experiments with help from AMJ, MW, ES and JMF. RK helped in the collection and interpretation of electron microscopy data. All authors contributed to revising the manuscript.

Conflict of interest

The authors declare no conflicts of interest.

References

Abdul Rahman, S., E. Bergstrom, C.J. Watson, K.M. Wilson, D.A. Ashford, J.R. Thomas, D. Ungar, and J. Thomas-Oates. 2014. Filter-Aided *N*-Glycan Separation (FANGS): a Convenient Sample Preparation Method for Mass Spectrometric *N*-Glycan Profiling. *J Proteome Res*. 13:1167–1176.

Alisson-Silva, F., D. de Carvalho Rodrigues, L. Vairo, K.D. Asensi, A. Vasconcelos-dos-Santos, N.R. Mantuano, W.B. Dias, E. Rondinelli, R.C. Goldenberg, T.P. Urmenyi, and A.R. Todeschini. 2014. Evidences for the involvement of cell surface glycans in stem cell pluripotency and differentiation. *Glycobiology*. 24:458-468.

An, H.J., P. Gip, J. Kim, S. Wu, K.W. Park, C.T. McVaugh, D.V. Schaffer, C.R. Bertozzi, and C.B. Lebrilla. 2012. Extensive determination of glycan heterogeneity reveals an unusual abundance of high mannose glycans in enriched plasma membranes of human embryonic stem cells. *Mol Cell Proteomics*. 11:M111.010660.

Bailey Blackburn, J., I. Pokrovskaya, P. Fisher, D. Ungar, and V.V. Lupashin. 2016. COG Complex Complexities: Detailed Characterization of a Complete Set of HEK293T Cells Lacking Individual COG Subunits. *Front Cell Dev Biol*. 4:23.

Belloni, G., S. Sechi, M.G. Riparbelli, M.T. Fuller, G. Callaini, and M.G. Giansanti. 2012. Mutations in Cog7 affect Golgi structure, meiotic cytokinesis and sperm development during Drosophila spermatogenesis. *J. Cell Sci.* doi: 10.1242/jcs.108878.

Chatzipanagis, K., M. Iafisco, T. Roncal-Herrero, M. Bilton, A. Tampieri, R. Kroger, and J.M. Delgado-Lopez. 2016. Crystallization of citrate-stabilized amorphous calcium phosphate to nanocrystalline apatite: a surface-mediated transformation. *Crystengcomm*. 18:3170-3173.

Coman, D., M. Irving, P. Kannu, J. Jaeken, and R. Savarirayan. 2008. The skeletal manifestations of the congenital disorders of glycosylation. *Clin Genet*. 73:507-515.

Cook, D., and P. Genever. 2013. Regulation of mesenchymal stem cell differentiation. *Adv Exp Med Biol*. 786:213-229.

Drickamer, K. 1992. Engineering galactose-binding activity into a C-type mannose-binding protein. *Nature*. 360:183-186.

Ducy, P., R. Zhang, V. Geoffroy, A.L. Ridall, and G. Karsenty. 1997. Osf2/Cbfa1: a transcriptional activator of osteoblast differentiation. *Cell*. 89:747-754.

Elbein, A.D., J.E. Tropea, M. Mitchell, and G.P. Kaushal. 1990. Kifunensine, a potent inhibitor of the glycoprotein processing mannosidase I. *J. Biol. Chem.* 265:15599-15605.

Fisher, P., and D. Ungar. 2016. Bridging the Gap between Glycosylation and Vesicle Traffic. *Front Cell Dev Biol*. 4:15.

Franke, T.F., S.I. Yang, T.O. Chan, K. Datta, A. Kazlauskas, D.K. Morrison, D.R. Kaplan, and P.N. Tsichlis. 1995. The protein kinase encoded by the Akt proto-oncogene is a target of the PDGF-activated phosphatidylinositol 3-kinase. *Cell*. 81:727-736.

Ghosh-Choudhury, N., S.L. Abboud, R. Nishimura, A. Celeste, L. Mahimainathan, and G.G. Choudhury. 2002. Requirement of BMP-2-induced phosphatidylinositol 3-kinase and Akt serine/threonine kinase in osteoblast differentiation and Smad-dependent BMP-2 gene transcription. *J Biol Chem*. 277:33361-33368.

Gross, V., T.A. Tran-Thi, K. Vosbeck, and P.C. Heinrich. 1983. Effect of swainsonine on the processing of the asparagine-linked carbohydrate chains of alpha 1-antitrypsin in rat hepatocytes. Evidence for the formation of hybrid oligosaccharides. *J. Biol. Chem.* 258:4032-4036.

Hamidouche, Z., O. Fromigue, J. Ringe, T. Haupl, P. Vaudin, J.C. Pages, S. Srouji, E. Livne, and P.J. Marie. 2009. Priming integrin alpha5 promotes human mesenchymal stromal cell osteoblast differentiation and osteogenesis. *Proc Natl Acad Sci U S A*. 106:18587-18591.

Hamouda, H., M. Ullah, M. Berger, M. Sittinger, R. Tauber, J. Ringe, and V. Blanchard. 2013. N-glycosylation profile of undifferentiated and adipogenically differentiated human bone marrow mesenchymal stem cells: towards a next generation of stem cell markers. *Stem Cells Dev*. 22:3100-3113.

Hasehira, K., H. Tateno, Y. Onuma, Y. Ito, M. Asashima, and J. Hirabayashi. 2012. Structural and quantitative evidence for dynamic glycome shift on production of induced pluripotent stem cells. *Mol Cell Proteomics*. 11:1913-1923.

Hennet, T., and J. Cabalzar. 2015. Congenital disorders of glycosylation: a concise chart of glycocalyx dysfunction. *Trends Biochem Sci*. 40:377-384.

Ihrke, G., J.R. Bruns, J.P. Luzio, and O.A. Weisz. 2001. Competing sorting signals guide endolyn along a novel route to lysosomes in MDCK cells. *EMBO J*. 20:6256-6264.

James, S., J. Fox, F. Afsari, J. Lee, S. Clough, C. Knight, J. Ashmore, P. Ashton, O. Preham, M. Hoogduijn, A. Ponzoni Rde, Y. Hancock, M. Coles, and P. Genever. 2015. Multiparameter Analysis

of Human Bone Marrow Stromal Cells Identifies Distinct Immunomodulatory and Differentiation-Competent Subtypes. *Stem Cell Reports*. 4:1004-1015.

Kingsley, D.M., K.F. Kozarsky, M. Segal, and M. Krieger. 1986. Three types of low density lipoprotein receptor-deficient mutant have pleiotropic defects in the synthesis of N-linked, O-linked, and lipid-linked carbohydrate chains. *J. Cell Biol.* 102:1576-1585.

Kratchmarova, I., B. Blagoev, M. Haack-Sorensen, M. Kassem, and M. Mann. 2005. Mechanism of divergent growth factor effects in mesenchymal stem cell differentiation. *Science*. 308:1472-1477.

Kuan, S.F., J.C. Byrd, C. Basbaum, and Y.S. Kim. 1989. Inhibition of mucin glycosylation by aryl-N-acetyl-alpha-galactosaminides in human colon cancer cells. *J Biol Chem*. 264:19271-19277.

Kulterer, B., G. Friedl, A. Jandrositz, F. Sanchez-Cabo, A. Prokesch, C. Paar, M. Scheideler, R. Windhager, K.H. Preisegger, and Z. Trajanoski. 2007. Gene expression profiling of human mesenchymal stem cells derived from bone marrow during expansion and osteoblast differentiation. *BMC Genomics*. 8:70.

Kumar, A., T. Torii, Y. Ishino, D. Muraoka, T. Yoshimura, A. Togayachi, H. Narimatsu, K. Ikenaka, and S. Hitoshi. 2013. The Lewis X-related alpha1,3-fucosyltransferase, Fut10, is required for the maintenance of stem cell populations. *J. Biol. Chem.* 288:28859-28868.

Kumarasuriyar, A., I. Lee, V. Nurcombe, and S.M. Cool. 2009. De-sulfation of MG-63 cell glycosaminoglycans delays in vitro osteogenesis, up-regulates cholesterol synthesis and disrupts cell cycle and the actin cytoskeleton. *J Cell Physiol*. 219:572-583.

Lau, K.S., E.A. Partridge, A. Grigorian, C.I. Silvescu, V.N. Reinhold, M. Demetriou, and J.W. Dennis. 2007. Complex N-glycan number and degree of branching cooperate to regulate cell proliferation and differentiation. *Cell*. 129:123-134.

Lee, K.S., H.J. Kim, Q.L. Li, X.Z. Chi, C. Ueta, T. Komori, J.M. Wozney, E.G. Kim, J.Y. Choi, H.M. Ryoo, and S.C. Bae. 2000. Runx2 is a common target of transforming growth factor beta1 and bone morphogenetic protein 2, and cooperation between Runx2 and Smad5 induces osteoblast-specific gene expression in the pluripotent mesenchymal precursor cell line C2C12. *Mol Cell Biol*. 20:8783-8792.

Lin, C.R., T.Y. Wei, H.Y. Tsai, Y.T. Wu, P.Y. Wu, and S.T. Chen. 2015. Glycosylation-dependent interaction between CD69 and S100A8/S100A9 complex is required for regulatory T-cell differentiation. *FASEB J*. 29:5006-5017.

Ling, L., C. Dombrowski, K.M. Foong, L.M. Haupt, G.S. Stein, V. Nurcombe, A.J. van Wijnen, and S.M. Cool. 2010. Synergism between Wnt3a and heparin enhances osteogenesis via a phosphoinositide 3-kinase/Akt/RUNX2 pathway. *J Biol Chem*. 285:26233-26244.

Miller, V.J., P. Sharma, T.A. Kudlyk, L. Frost, A.P. Rofe, I.J. Watson, R. Duden, M. Lowe, V.V. Lupashin, and D. Ungar. 2013. Molecular insights into vesicle tethering at the Golgi by the Conserved Oligomeric Golgi (COG) complex and the golgin TMF. *J Biol Chem*. 288:4229-4240.

Miller, V.J., and D. Ungar. 2012. Re'COG'nition at the Golgi. *Traffic*. 13:891-897.

Moody, A.M., D. Chui, P.A. Reche, J.J. Priatel, J.D. Marth, and E.L. Reinherz. 2001. Developmentally regulated glycosylation of the CD8alphabeta coreceptor stalk modulates ligand binding. *Cell*. 107:501-512.

Oka, T., D. Ungar, F.M. Hughson, and M. Krieger. 2004. The COG and COPI complexes interact to control the abundance of GEARs, a subset of Golgi integral membrane proteins. *Mol. Biol. Cell*. 15:2423-2435.

Partridge, E.A., C. Le Roy, G.M. Di Guglielmo, J. Pawling, P. Cheung, M. Granovsky, I.R. Nabi, J.L. Wrana, and J.W. Dennis. 2004. Regulation of cytokine receptors by Golgi N-glycan processing and endocytosis. *Science*. 306:120-124.

Quarto, N., B. Behr, and M.T. Longaker. 2010. Opposite spectrum of activity of canonical Wnt signaling in the osteogenic context of undifferentiated and differentiated mesenchymal cells: implications for tissue engineering. *Tissue Eng Part A*. 16:3185-3197.

Rubin, M.A., I. Jasiuk, J. Taylor, J. Rubin, T. Ganey, and R.P. Apkarian. 2003. TEM analysis of the nanostructure of normal and osteoporotic human trabecular bone. *Bone*. 33:270-282.

Sasaki, N., M. Shinomi, K. Hirano, K. Ui-Tei, and S. Nishihara. 2011. LacdiNAc (GalNAc beta 1-4GlcNAc) Contributes to Self-Renewal of Mouse Embryonic Stem Cells by Regulating Leukemia Inhibitory Factor/STAT3 Signaling. *Stem Cells*. 29:641-650.

Sato, Y., M. Takahashi, Y. Shibukawa, S.K. Jain, R. Hamaoka, J. Miyagawa, Y. Yaginuma, K. Honke, M. Ishikawa, and N. Taniguchi. 2001. Overexpression of N-acetylglucosaminyltransferase III enhances the epidermal growth factor-induced phosphorylation of ERK in HeLaS3 cells by up-regulation of the internalization rate of the receptors. *J Biol Chem*. 276:11956-11962.

Scott, D.W., T.S. Dunn, M.E. Ballestas, S.H. Litovsky, and R.P. Patel. 2013. Identification of a high-mannose ICAM-1 glycoform: effects of ICAM-1 hypoglycosylation on monocyte adhesion and outside in signaling. *Am J Physiol Cell Physiol*. 305:C228-237.

Skeene, K., M. Walker, G. Clarke, E. Bergstrom, P. Genever, D. Ungar, and J. Thomas-Oates. 2017. One Filter, One Sample, and the N- and O-Glyco(proteo)me: Toward a System to Study Disorders of Protein Glycosylation. *Anal Chem*. 89:5840-5849.

Spessott, W., A. Uliana, and H.J. Maccioni. 2010. Cog2 null mutant CHO cells show defective sphingomyelin synthesis. *J. Biol. Chem.* 285:41472-41482.

Struwe, W.B., and V.N. Reinhold. 2012. The conserved oligomeric Golgi complex is required for fucosylation of N-glycans in Caenorhabditis elegans. *Glycobiology*. 22:863-875.

Su, N., M. Jin, and L. Chen. 2014. Role of FGF/FGFR signaling in skeletal development and homeostasis: learning from mouse models. *Bone Res*. 2:14003.

Sykes, B., D. Ogilvie, P. Wordsworth, Anderson, and N. Jones. 1986. Osteogenesis imperfecta is linked to both type I collagen structural genes. *Lancet*. 2:69-72.

Tateno, H., S. Saito, K. Hiemori, K. Kiyoi, K. Hasehira, M. Toyoda, Y. Onuma, Y. Ito, H. Akutsu, and J. Hirabayashi. 2016. alpha2-6 sialylation is a marker of the differentiation potential of human mesenchymal stem cells. *Glycobiology*. 26:1328-1337.

Ungar, D. 2009. Golgi linked protein glycosylation and associated diseases. *Semin. Cell Dev. Biol.* 20:762-769.

Wang, Y., T. Azaïs, M. Robin, A. Vallée, C. Catania, P. Legriel, G. Pehau-Arnaudet, F. Babonneau, M.-M. Giraud-Guille, and N. Nassif. 2012. The predominant role of collagen in the nucleation, growth, structure and orientation of bone apatite. *Nat Mater*. 11:724-733.

Weiner, S., and W. Traub. 1992. Bone-Structure - from Angstroms to Microns. *Faseb Journal*. 6:879-885.

Whyte, J.R.C., and S. Munro. 2001. The Sec34/35 Golgi Transport Complex is related to the exocyst, defining a family of complexes involved in multiple steps of membrane traffic. *Dev. Cell*. 1:527-537.

Wilson, K.M., J.E. Thomas-Oates, P.G. Genever, and D. Ungar. 2016. Glycan Profiling Shows Unvaried N-Glycomes in MSC Clones with Distinct Differentiation Potentials. *Front Cell Dev Biol*. 4:52.

Wu, X., R.A. Steet, O. Bohorov, J. Bakker, J. Newell, M. Krieger, L. Spaapen, S. Kornfeld, and H.H. Freeze. 2004. Mutation of the COG complex subunit gene COG7 causes a lethal congenital disorder. *Nat. Med.* 10:518-523.

Yokota, J., N. Chosa, S. Sawada, N. Okubo, N. Takahashi, T. Hasegawa, H. Kondo, and A. Ishisaki. 2014. PDGF-induced PI3K-mediated signaling enhances the TGF-beta-induced osteogenic differentiation of human mesenchymal stem cells in a TGF-beta-activated MEK-dependent manner. *Int J Mol Med*. 33:534-542.

Yue, R., B. Shen, and S.J. Morrison. 2016. Clec11a/osteolectin is an osteogenic growth factor that promotes the maintenance of the adult skeleton. *Elife*. 5.

Figures

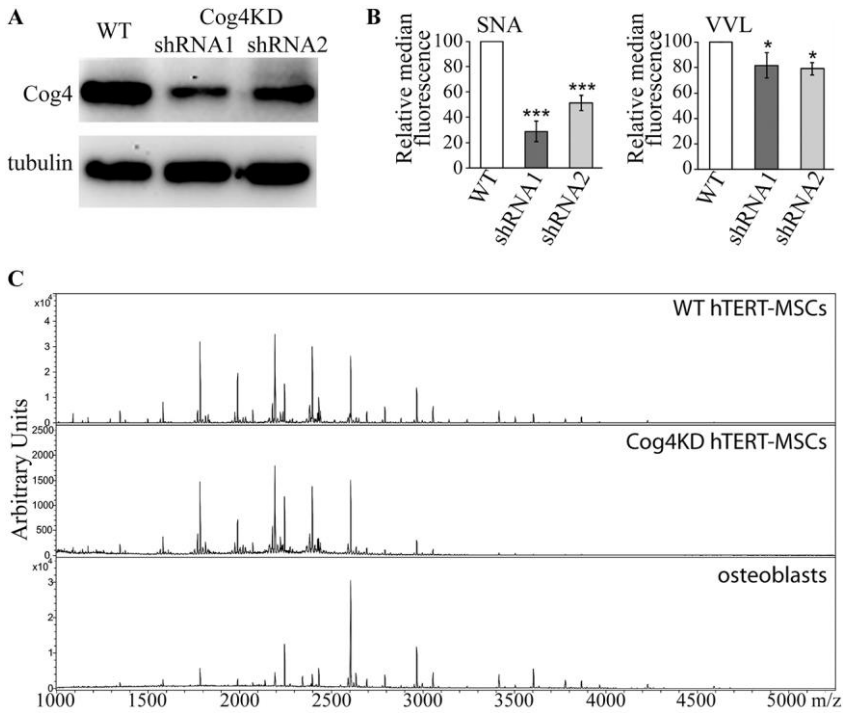

Figure 1. Cog4 knock-down in MSCs causes glycosylation defects.

(A) Immunoblot of WT and Cog4KD Y101 hTERT-MSC lysates probed for Cog4. Anti-tubulin was used as a loading control. (B) WT and Cog4KD Y101 hTERT-MSCs were stained with 10 µg/mL FITC-tagged VVL or 10 µg/mL biotin-labelled SNA followed by 5 µg/mL FITC-streptavidin, and the fluorescence intensity of 10^5 cells measured by FACS. Shown are the median fluorescence intensities of the KD cell lines relative to WT. Error bars display SEM for n=3. (C) Mass spectrometric *N*-glycan profiles of FANGS-released *N*-glycans from WT (top), Cog4KD (shRNA1, middle) Y101 hTERT-MSCs and osteoblasts derived from Y101 hTERT-MSCs (bottom). Detailed annotated spectra of the WT and osteoblast lines have been published in (Wilson et al., 2016), and are reproduced here to serve as a comparison for the Cog4KD cells.

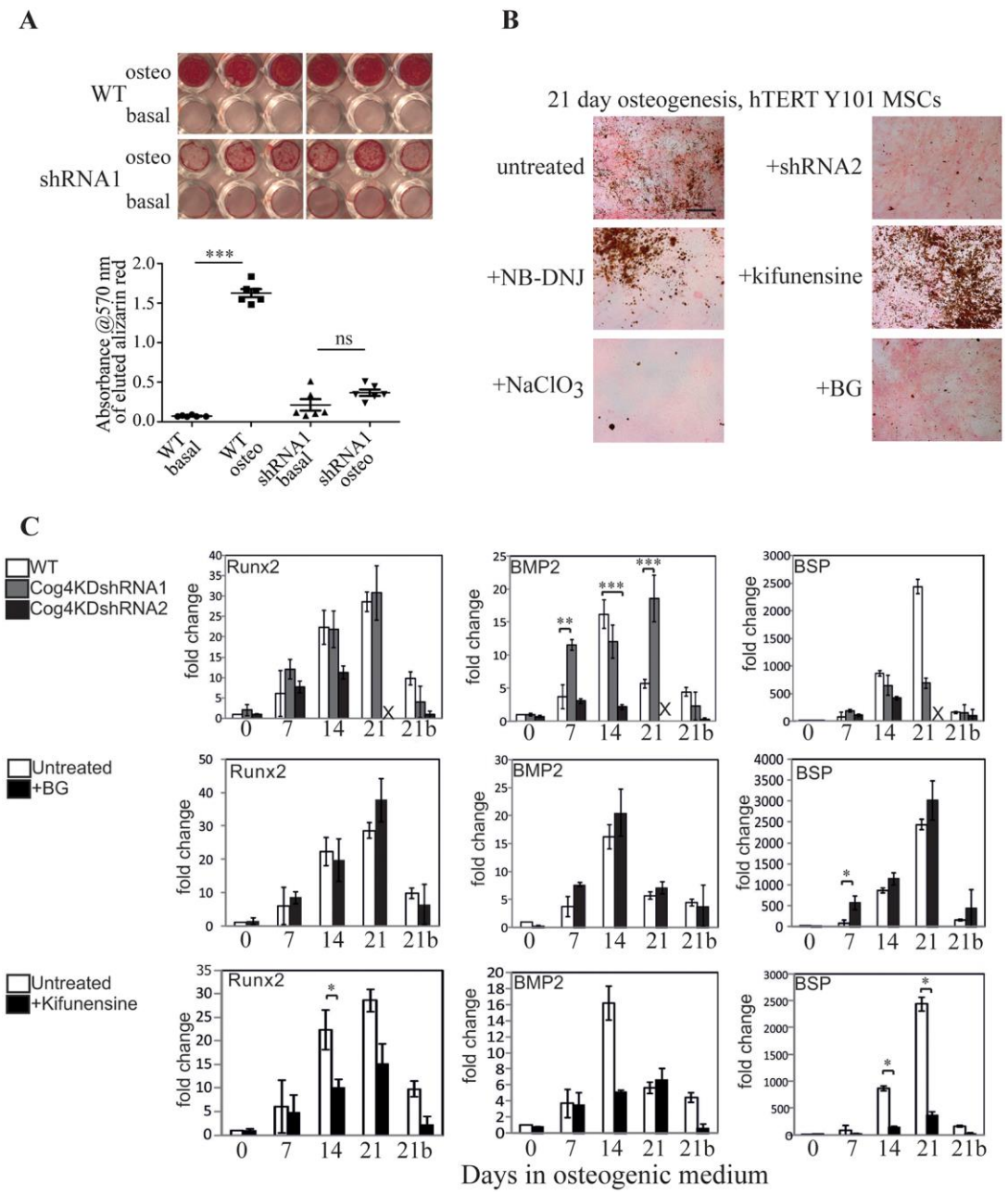

Figure 2. Altered glycan processing affects the function of MSC derived osteoblasts.

(A) Alizarin red staining of WT or Cog4KD Y101 hTERT-MSC cells following a 21 day differentiation experiment in osteogenic medium. Quantification of the eluted alizarin red stain is shown in the graph below the image. Error bars show standard deviation for n=6. (B) ALP/von Kossa staining of Y101 cells or Y101 cells stably expressing a Cog4 specific shRNA (shRNA2) following incubations in osteogenic medium with the indicated inhibitors for 21 days. NB-DNJ: *N*-butyldeoxynojirimycin, BG: benzyl-O-GalNAc. Scale bar is 100 µm. (C) Quantitative real-time PCR analysis of mRNA expression levels of indicated genes

in the Y101 WT or shRNA KD cells. Medium was supplemented with the indicated inhibitors two days prior to the start of and until the end of the differentiation experiments. Averages of triplicate measurements were normalized to the day zero control. Data represent averages of averages of three technical repeats each for two independent biological replicates (each normalized independently to its own control) with SEM shown. The bar positions marked with 'X' are from the 21 day shRNA2 samples that peeled off. All qPCR experiments in Fig 2C and 3B were performed in parallel, and used the same untreated WT as control. This control is replicated in all three rows of 2C as well as 3B for clarity. All significant differences compared to the control samples are marked with asterisks, all other changes are non-significant.

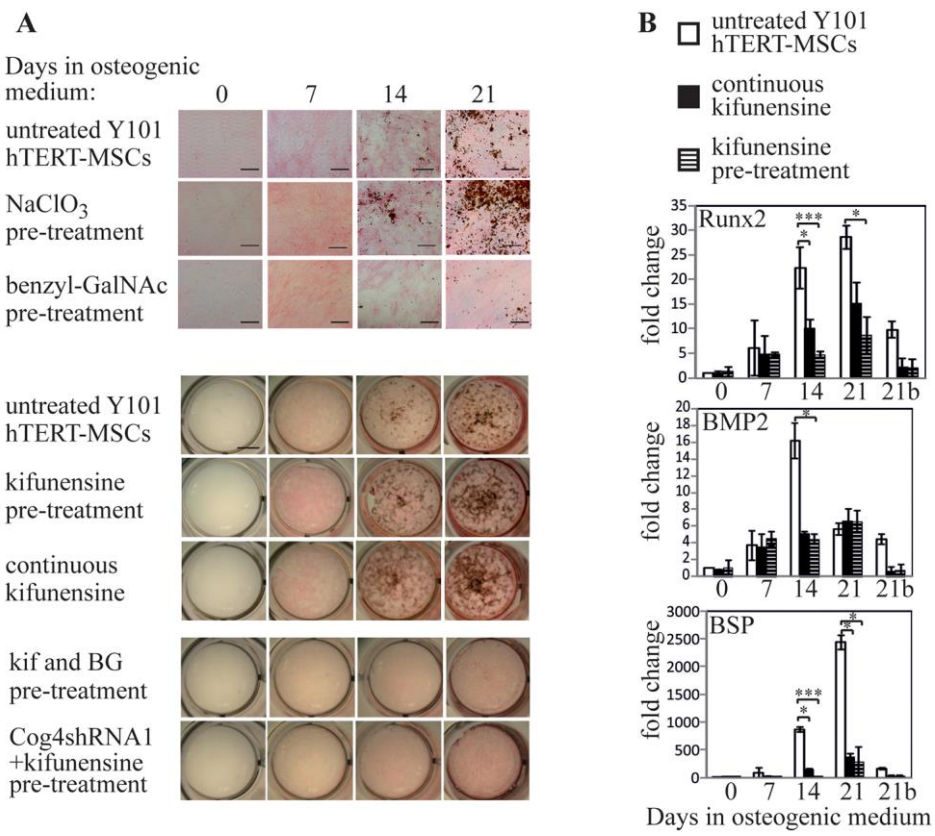

Figure 3. *N*- and O-glycan processing mediate early steps in differentiation.

(A) WT Y101 hTERT-MSCs were pre-treated with the indicated inhibitors for 48 h before differentiation was induced in osteogenic medium in the absence of inhibitors for 21 days (inhibitors were included for the full 21 days for comparison where indicated as 'continuous'). ALP/von Kossa staining was performed on the indicated days. The images in the last row show Cog4KD cells rather than WT. Scale bar 100 µm for the top three rows, 5 mm for the bottom five rows. (B) Quantitative real-time PCR experiments performed as in Fig 2C with Y101 cells cultured in osteogenic medium in the continuous presence of kifunensine following a 48 h pre-treatment or pre-treated with kifunensine for 48 h followed by incubation in medium without kifunensine. The +kif data are repeated from Fig 2 for clarity. All significant differences compared to the control samples are marked with asterisks, all other changes are non-significant. Data represent averages of averages of three technical repeats each for two independent biological replicates with SEM shown.

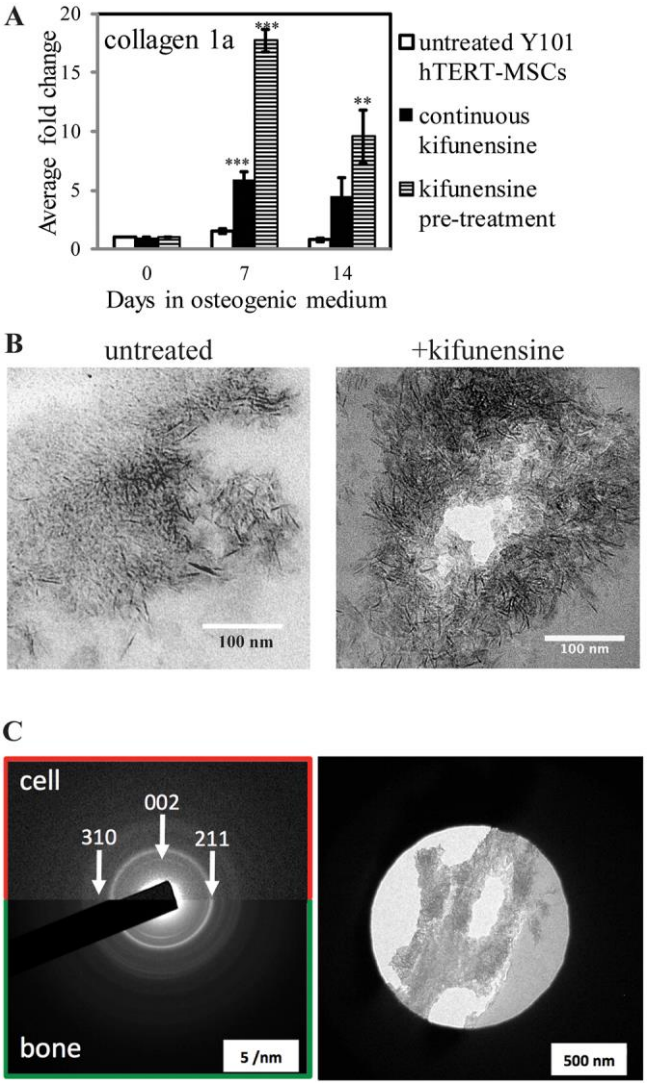

Figure 4. Mineralization enhancement by kifunensine yields well-structured mineral deposits.

(A) Quantitative real-time PCR analysis of collagen type 1 gene expression in Y101 cells incubated in osteogenic medium with the indicated inhibitor treatments. Experiments performed as for Fig 2C, but for 14 days only. (B) Transmission electron micrographs of 90 nm thin sections prepared from Epon Araldite embedded Y101 cell samples following 21 days of osteogenic differentiation. Kifunensine treatment was for 48 h prior to start of differentiation only. (C) Electron diffraction images of a bone sample (bottom half) and a sample of the resin embedded Y101 cells differentiated following kifunensine pre-treatment (top half). The positions of three diffraction rings characteristic for hydroxyapatite are indicated with arrows. The diffraction image of the cells was taken from the region shown in the right side panel.

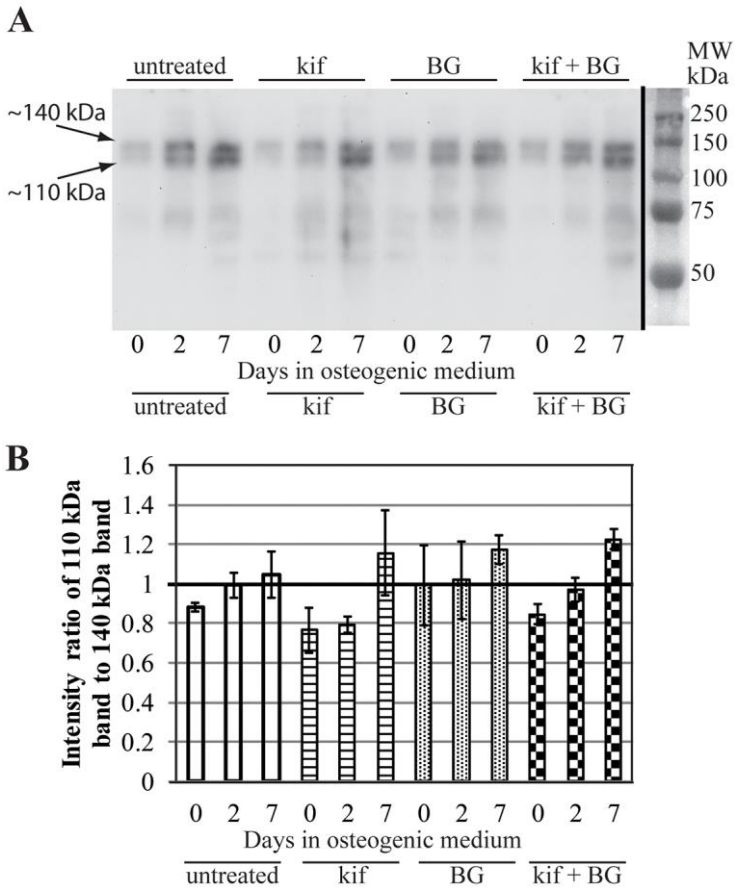

Figure 5. Altered phosphotyrosine signalling early in osteogenesis upon kifunensine treatment.

(A) Y101 cells cultured in osteogenic medium for 0, 2, 7 days were treated with the indicated inhibitors for 48 h prior to the start of differentiation. Total cell lysates were separated on 10% SDS-PAGE and immunoblots probed with the phosophotyrosine specific PY20 antibody. (B) The intensities of the two major bands between the 100 and 150 kDa molecular weight markers (marked with arrows, with the apparent molecular weights indicated) were quantified using ImageJ, and their ratio charted. Error bars show SEM for two independent experiments.

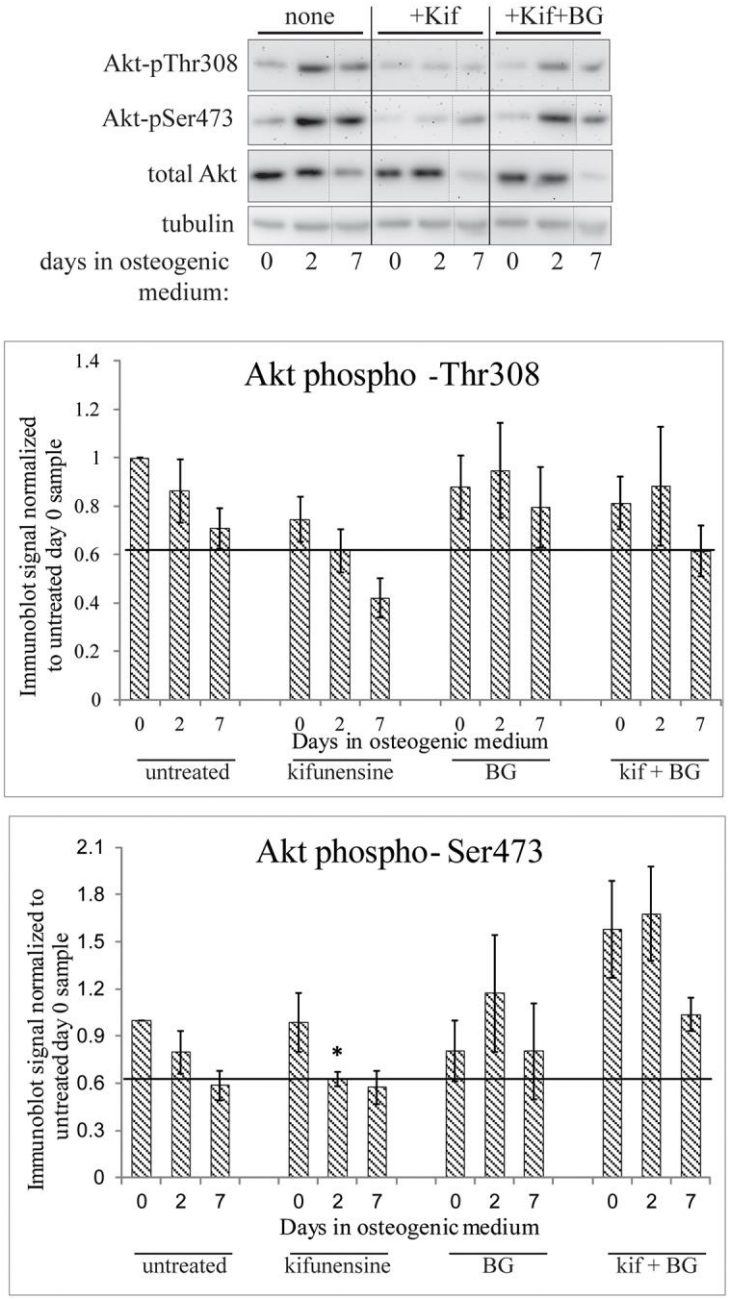

Figure 6. Altered Akt/PKB activation during early osteogenic differentiation following kifunensine treatment.

Cell lysates prepared as in Fig 5A were immunoblotted for total Akt as well as for Thr308 and Ser473 phosphorylation on Akt. Band intensities were quantified by ImageJ and averaged following normalization of the phosphorylation-specific signals to the tubulin and total Akt signals, followed by normalization to the day zero untreated sample. Dotted lines indicate where the blot was cut and pasted to move two lanes from the same blot next to each

other. All bands shown in one row are taken from the same image. Horizontal lines in the bar charts were drawn to highlight the levels of phospho-Akt in kifunensine pre-treated day 2 samples. Error bars show SEM for n=4 (all pThr308 samples), n=6 (untreated, kifunensine and BG treated pSer473 samples), n=3 (double treated pSer473 samples). Asterisk marks the statistically significant reduction of pSer473 staining in the kifunensine treated day 2 sample.

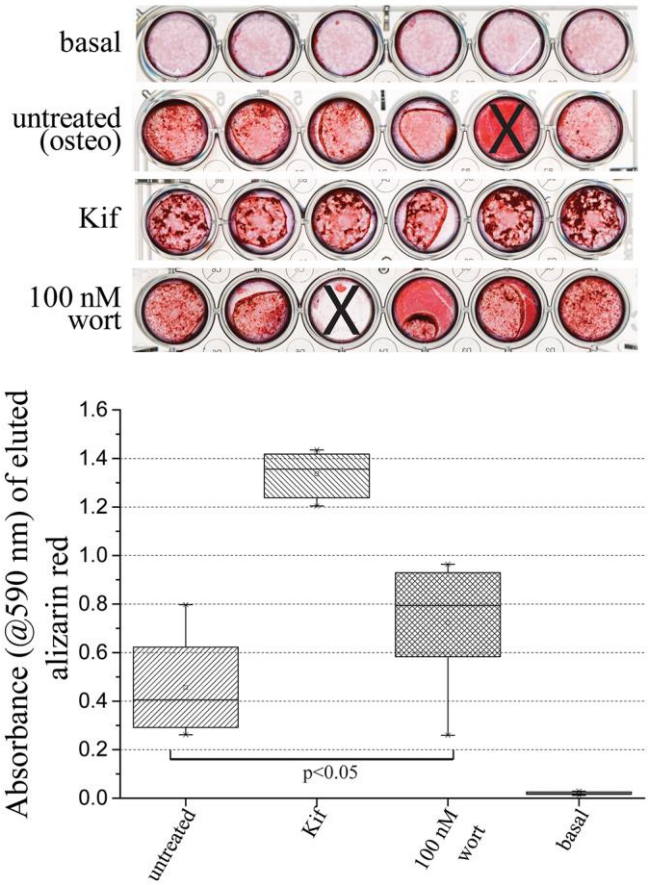

Figure 7. PI3K inhibition can phenocopy kifunensine treatment.

Y101 cells were grown in osteogenic medium or control basal medium for 21 days and stained with alizarin red. Cells were either untreated, pre-treated with kifunensine for 48 hours, or treated with 100 nM wortmannin for the first two days of the differentiation period. Images of representative stained wells are shown below the quantification of the eluted alizarin. SEM for n=8 (n=6 for untreated). Asterisks mark statistically significant differences.

Wilson et al.
Supplementary Figure 1.

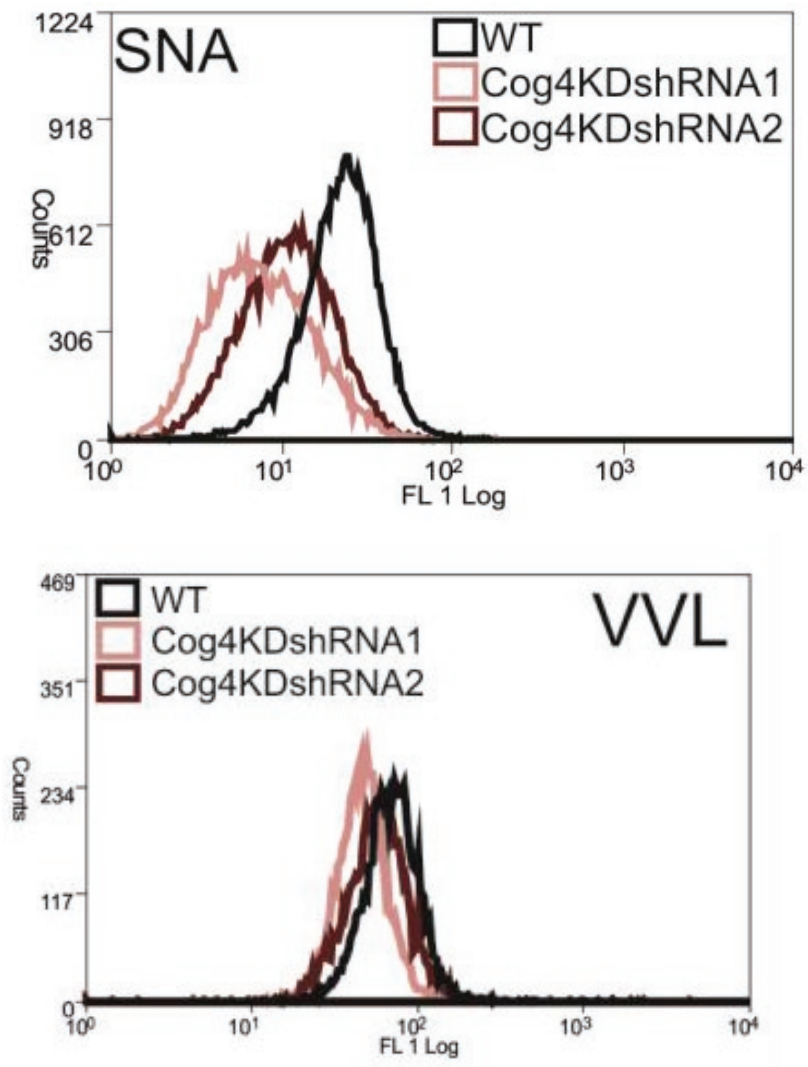

Supplementary Figure 1. Glycan analysis of Cog4KD cells using fluorescent lectins.
WT (black), Cog4KDshRNA1 (pink) and Cog4KDshRNA2 (brown) Y101 hTERT-MSCs were probed with SNA (top) and VVL (bottom) lectins. Histograms show cell counts versus log FITC fluorescence.

Wilson et al.
Supplementary Figure 2

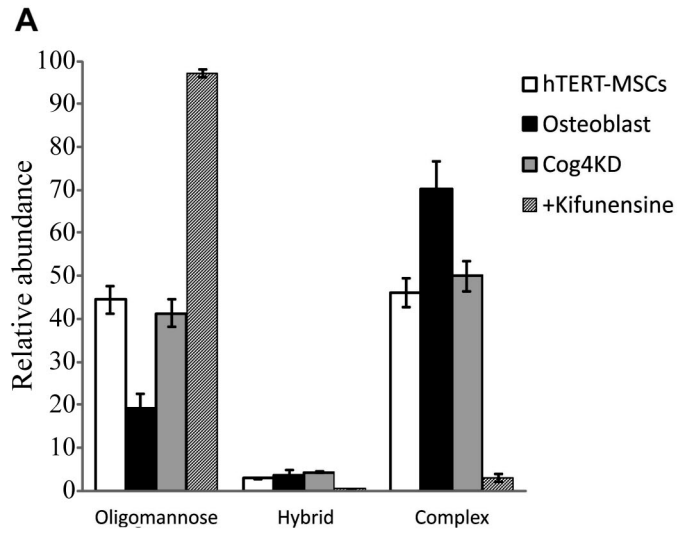

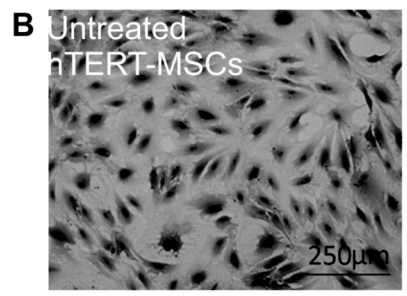

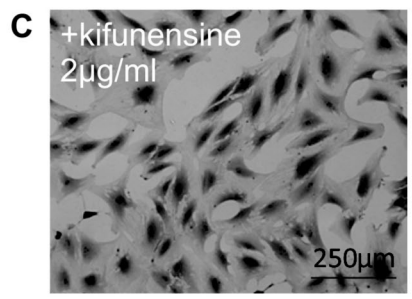

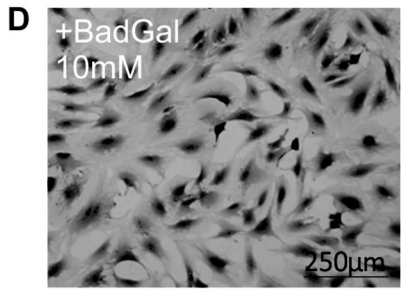

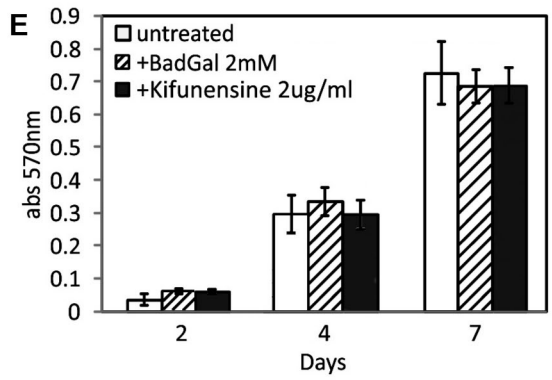

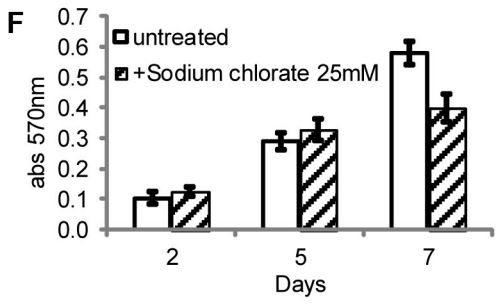

Supplementary Figure 2. Effects of glycan processing inhibitors on glycans and cell proliferation in Y101 hTERT MSCs.
(A) Quantification of glycan classes in the *N*-glycan profiles of WT, Cog4KD and osteogenically differentiated Y101 hTERT-MSCs as well as WT cells treated with kifunensine. Error bars are SEM for n=5 (hTERT-MSC) or n=3 (all others). The WT and osteoblast *N*-glycan quantifications have been published in (Wilson et al., 2016), and are reproduced here for comparison. (B-D) Bright-field images of cells stained with crystal violet following continuous treatment with the indicated inhibitor. (E-F) Results of MTT assays comparing untreated and continuously inhibitor treated cells.

Wilson et al.
Supplementary Figure 3.

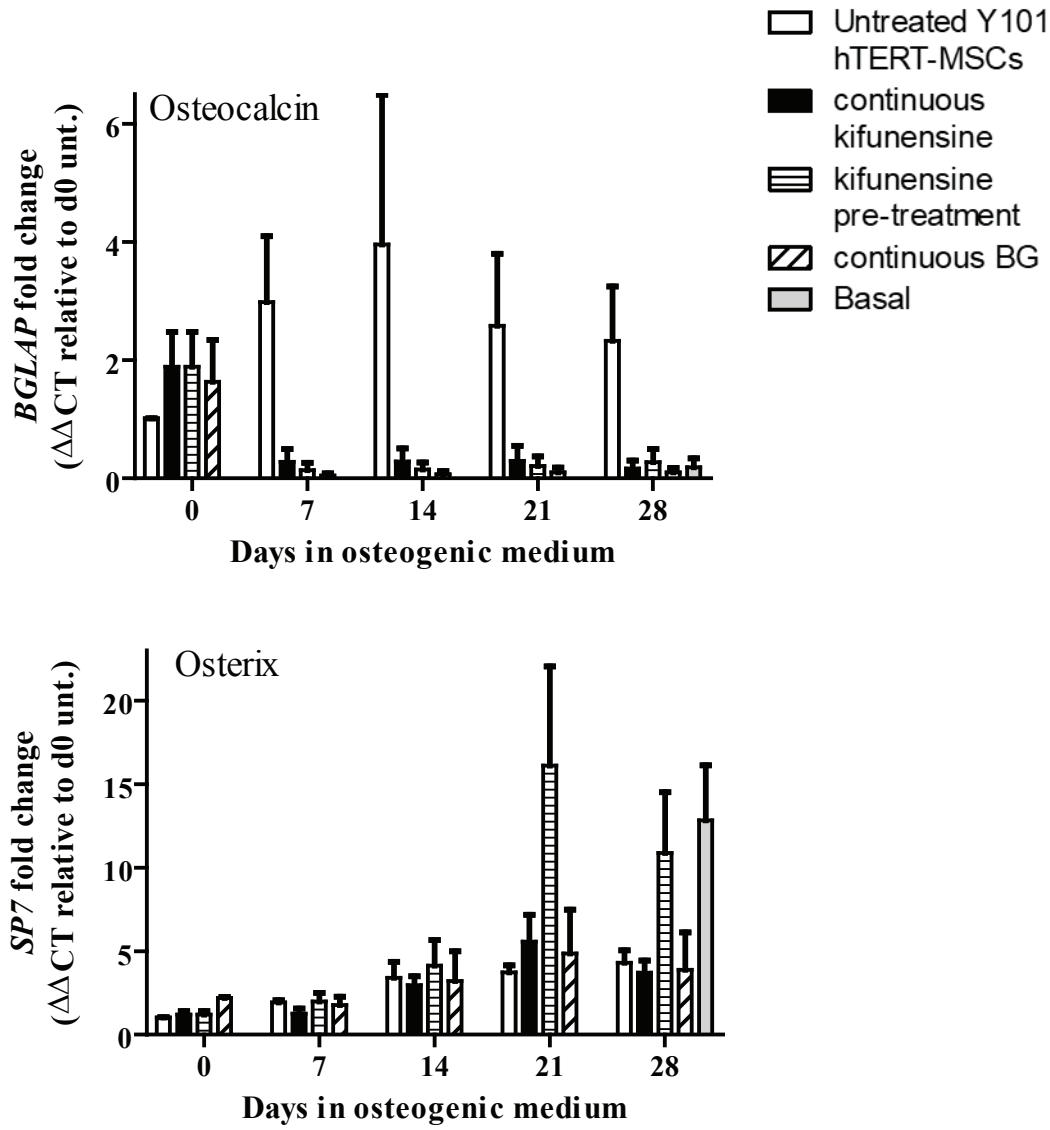

Supplementary Figure 3. Analysis of early and late differentiation markers in drug treated cells during osteogenic differentiation.
Quantitative real-time PCR analysis of mRNA expression levels of the early marker osterix and the late marker osteocalcin in Y101 hTERT-MSCs. Medium was supplemented with the indicated inhibitors two days prior to the start of differentiation, and where indicated continuously kept in the medium until the end of the differentiation experiments. Averages of triplicate measurements were normalized to the day zero control. The error bars are the SEM for three independent measurements, each normalized independently to its own control. None of the differences are statistically significant when the whole datasets are analysed. When samples are compared within a day the untreated samples are statistically significantly different from the drug treated ones on days 7 and 28 for osteocalcin.

Wilson et al
Supplementary Figure 4.

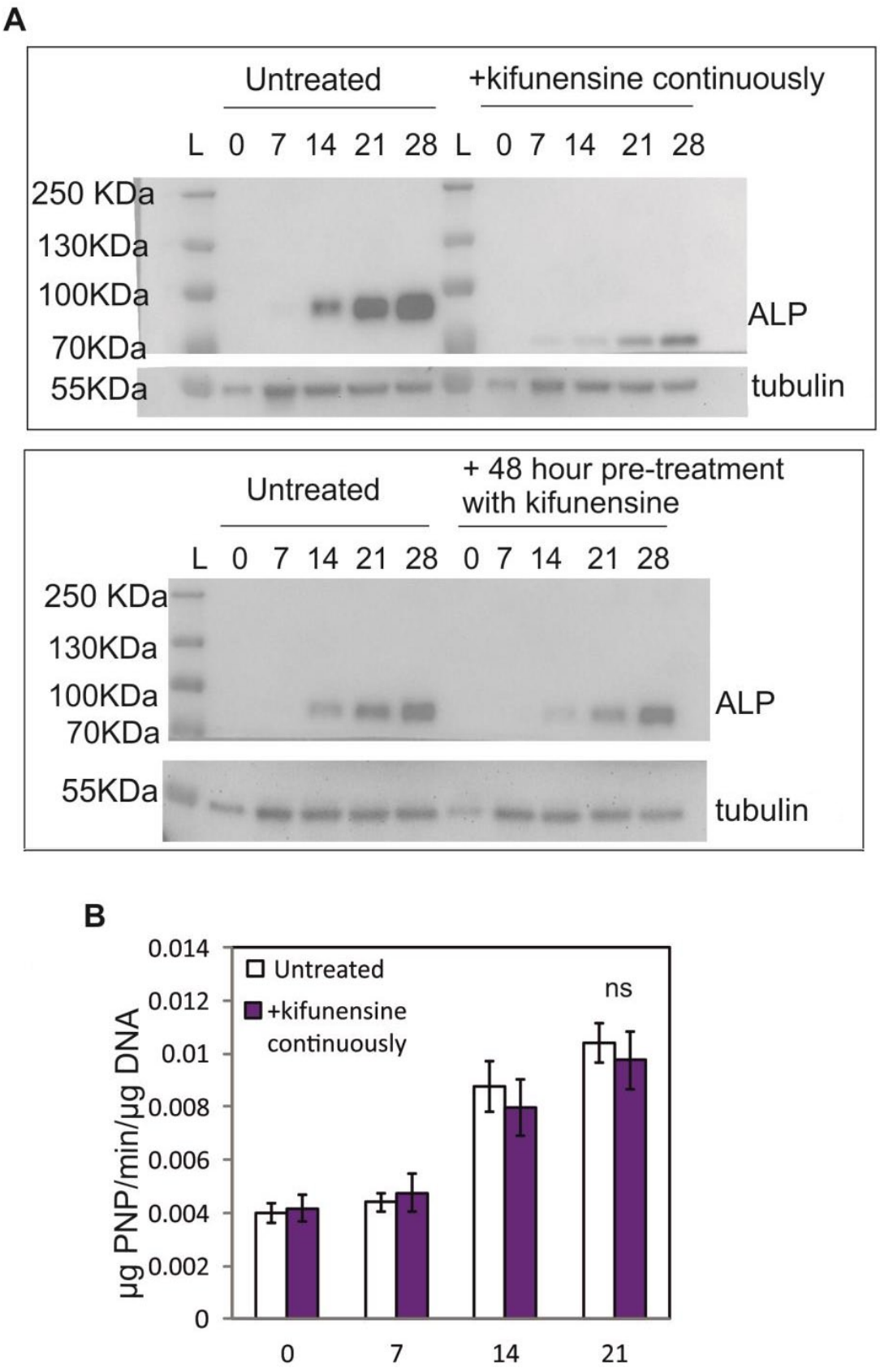

Supplementary Figure 4. Effect of kifunensine treatment on ALP activity and protein levels.
(A) Western blots of cells cultured in osteogenic medium for the indicated time and probed with anti-ALP antibody. Kifunensine treatment was continuous (top) or for 48 h pre-treatment only (bottom). Beta-tubulin was used as a loading control, L = protein molecular weight marker. (B) ALP activity inY101 cells cultured in osteogenic medium ±kifunensine for the indicated time was measured using pNP assay and normalized to DNA content determined using a pico-green assay. One way ANOVA, n=6, ns= non-significant, error bars show standard deviation.

Wilson et al.
Supplementary Figure 5

A

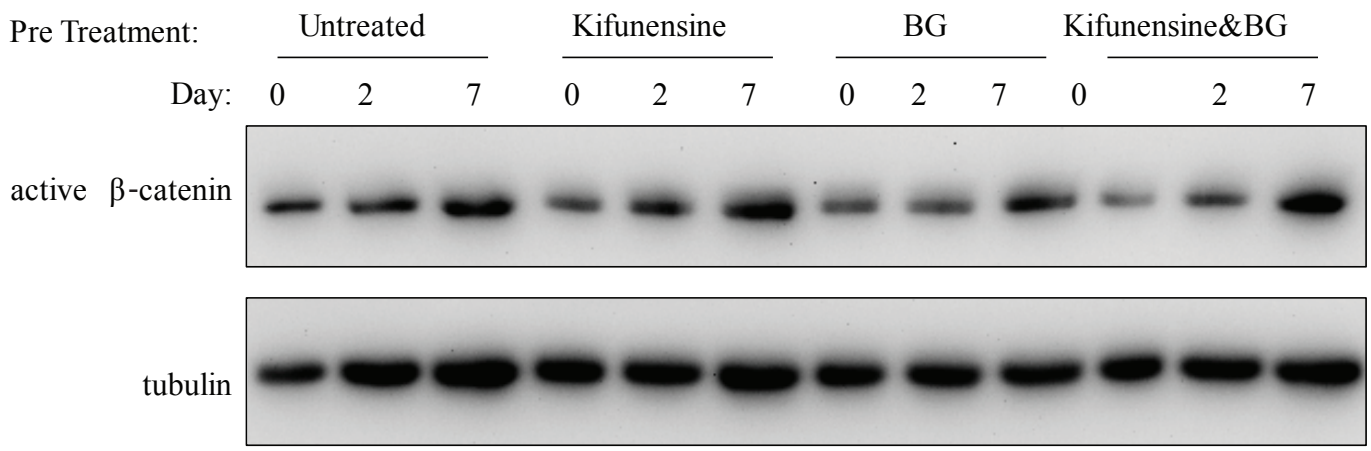

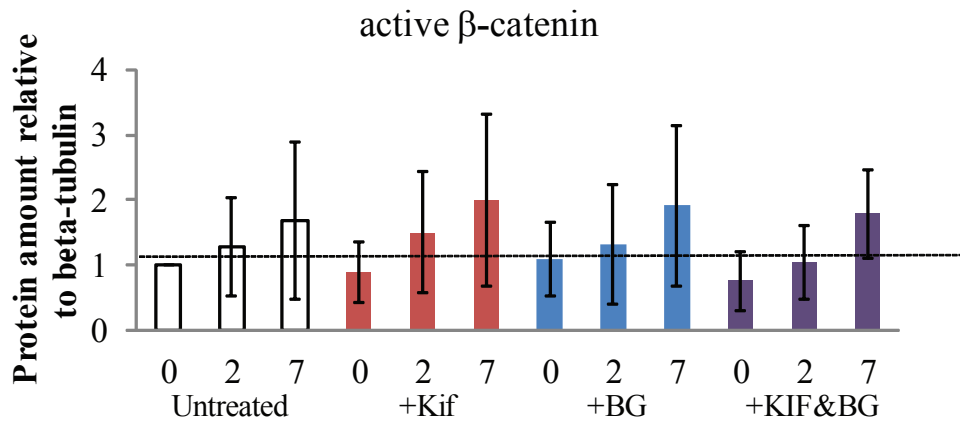

B

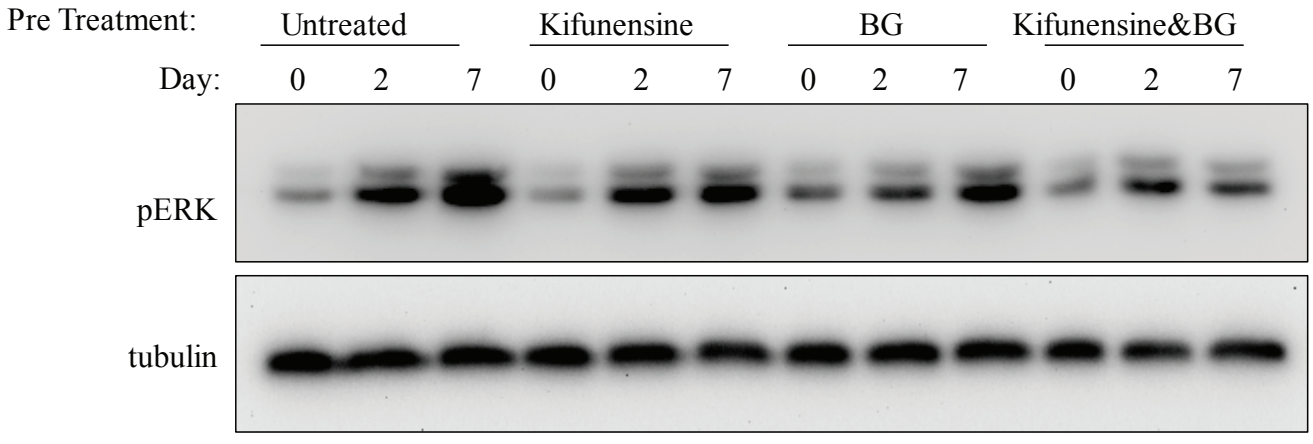

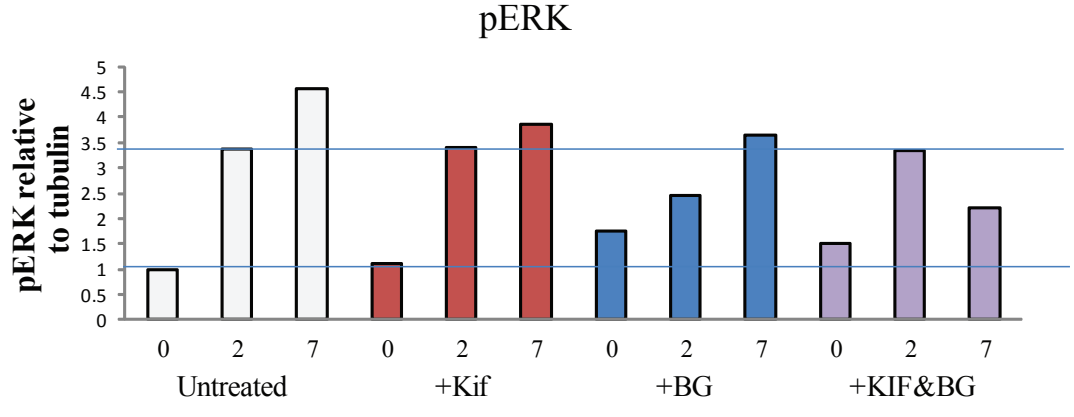

Supplementary Figure 5. Wnt/β-catenin and MAPK signalling are unperturbed by the tested glycosylation inhibitions during early osteogenesis.
Cells were grown and blotted as in Fig 5, β-tubulin was used as a loading control. Blots were probed for (A) active β-catenin (n=2) and (B) phosphorylated ERK (n=1).

Supplementary Figure 6. Wortmannin inhibition of PI3K during early osteogenesis.
Y101 hTERT-MSCs were cultured for 6 h in osteogenic medium in the presence or absence of 100 nM wortmannin and the phosphorylation state of Akt assessed (top). pAkt signals were quantified relative to the 0 h time-point run on the same gel following normalization to β-tubulin and total Akt levels. Error bars represent SEM for n=3 (S473) and n=6 (T308).

Wilson et al.
Supplementary Figure 6.

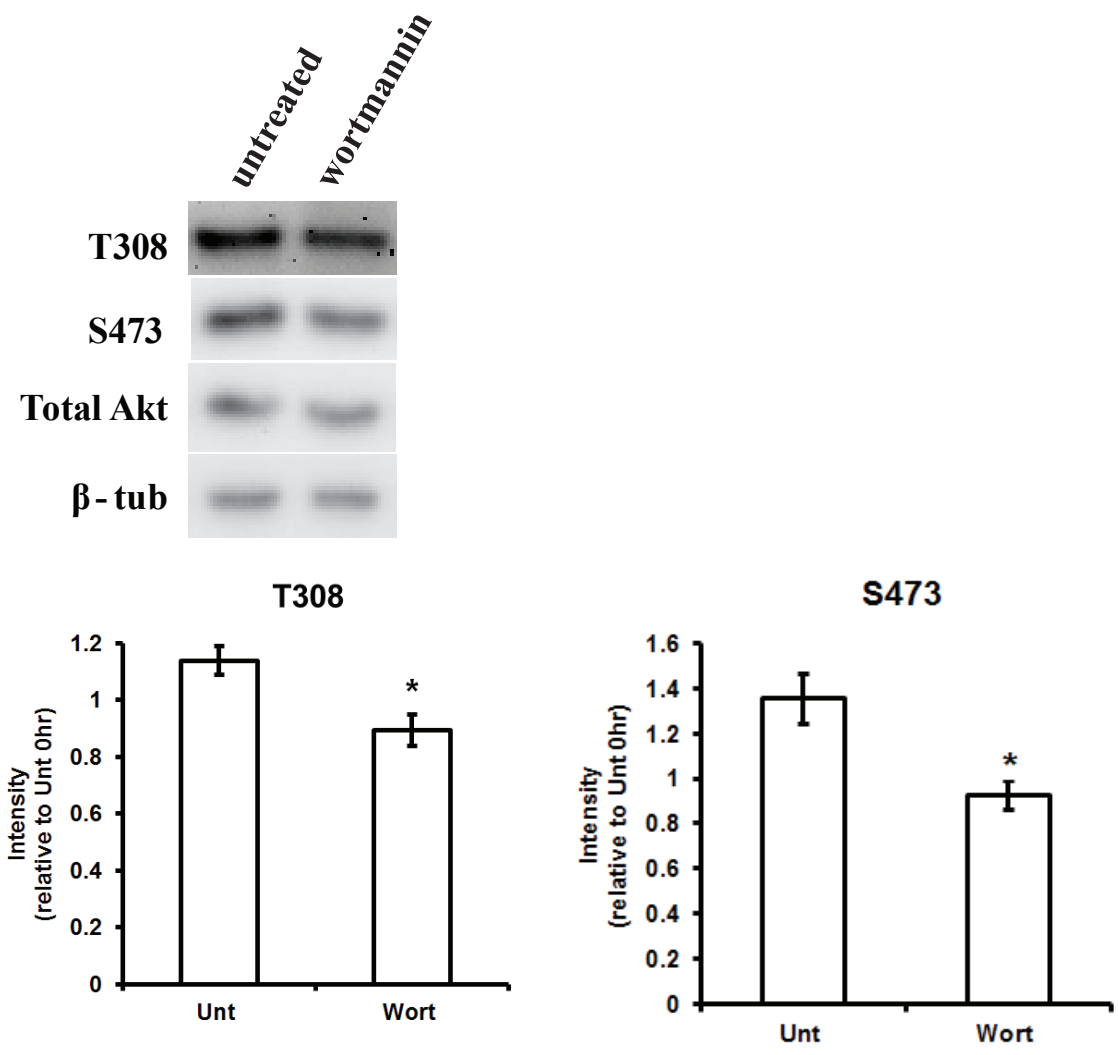

Supplementary Table 1. Comparison of averaged glycan abundances for the hTERT Y101 MSC and Cog4KD shRNA1 cells

Click here to Download Table S1